Journal of Pharmaceutical Sciences 111 (2022) 2093–2106

Contents lists available at ScienceDirect

Journal of Pharmaceutical Sciences

journal homepage: www.jpharmsci.org

Pharmacokinetics, Pharmacodynamics and Drug Transport and Metabolism

A Framework for Incorporating Transient Solute-Keratin Binding Into Dermal Absorption Models

Johannes M. Nitsche[a,*], Gerald B. Kasting[b]

[a] Department of Chemical and Biological Engineering, University at Buffalo, The State University of New York, Buffalo, NY 14260–4200, United States
[b] James L. Winkle College of Pharmacy, University of Cincinnati Academic Health Center, Cincinnati, OH 45267–0514, United States

ARTICLE INFO

Article history:
Received 19 August 2021
Revised 28 November 2021
Accepted 29 November 2021
Available online 19 February 2022

Keywords:
Skin
Transdermal
Passive diffusion
Membrane transport
Mathematical model
Protein binding
Membrane binding
Surface binding
Kinetics
Percutaneous

ABSTRACT

Interpretation of experiments involving transient solute binding to isolated keratin substrates is analyzed and discussed in terms of their impact on transient permeation of topically-applied compounds through human stratum corneum. The analysis builds upon an earlier model (Nitsche and Frasch 2011 Chem Eng Sci 66:2019-41) by adding a second level of homogenization (ultrascopic-to-microscopic) prior to the microscopic-to-macroscopic conversion. Here "ultrascopic" refers to isolated keratin suspensions, "microscopic" to corneocyte interiors and "macroscopic" to tissue-averaged properties in the stratum corneum. Results are interpreted in the context of current parameterizations of the underlying ultrascopic binding parameters. The present analysis, which is limited to linear binding isotherms common in dilute solutions, reveals a maximum in the macroscopic forward binding rate constant as a function of solute lipophilicity, whereas the underlying equilibrium constant increases monotonically and the macroscopic reverse binding rate constant decreases monotonically. The size and location of the maximum depends upon the hydration state of the stratum corneum. Explicit equations expressing these findings allow both equilibrium and kinetic binding data in isolated keratins to be applied to the kinetics of transient absorption through the skin. They will enable more quantitative estimation of the long-recognized stratum corneum reservoir function.

Introduction

Detailed mechanistic understanding of molecular absorption through the skin is critical to meeting the evolving demands of transdermal and topical drug development,[1–3] and risk assessment of chemical exposures.[4–6] This paper addresses an area of pressing need in these fields, namely the stark reality that dermal absorption models still cannot predict the time evolution of most drug/chemical applications and exposures to the skin, in part because the diffusional transients usually considered are inextricably intertwined with the kinetics of solute binding to intracellular keratin protein.[7–11] This phenomenon occurs ubiquitously on a time scale comparable to diffusion and has not been characterized in any comprehensive way. Thus, pivotally important parameters including lag time and the so-called reservoir capacity (or depot effect) of the stratum corneum (SC, barrier) layer of skin are as yet mired in uncertainty. A brief review of the multiscale architecture of this layer, as well as the current status of modeling and keratin binding studies, helps to frame the knowledge gap addressed.

Multiscale, Multiphase Architecture and Physicochemistry of the Stratum Corneum

The term "macroscopic" here refers to the scale at which the ~15 mm thickness of the SC, regarded as a homogeneous effective continuum, is discernible (Fig. 1(c)). For any given solute species, this layer is characterized by a partition coefficient $\overline{\overline{K}}^{sc/w}$ relative to an aqueous reference solution "w," diffusion coefficients $\overline{\overline{D}}^{sc}_{\perp}$ and $\overline{\overline{D}}^{sc}_{\parallel}$ for motions respectively perpendicular and parallel to the skin surface, and a (per-volume) rate expression for binding of solute to the tissue. At low concentrations this rate expression takes the form $\overline{\overline{k}}^{sc}_{on}\overline{\overline{C}}^{sc} - \overline{\overline{k}}^{sc}_{off}\overline{\overline{B}}^{sc}$ describing linear reversible binding. Here $\overline{\overline{C}}^{sc}$ and $\overline{\overline{B}}^{sc}$ represent the macroscopic average (superficial) concentrations of unbound (free, dissolved, mobile, diffusible) and bound (immobile) solute, and the two coefficients multiplying them represent "on" (binding) and "off" (unbinding) rate constants, respectively. All listed coefficients are effective (homogenized, coarse-grained) attributes of the tissue representing average outcomes of transport processes occurring within its two-phase microstructure, and are distinguished by a double overbar (=) affix.

* Corresponding author.
E-mail address: nitsche@buffalo.edu (J.M. Nitsche).

https://doi.org/10.1016/j.xphs.2021.11.026
0022-3549/

Nomenclature

Roman letters

a	radius (of keratin microfibril or solute molecule)
C	unbound (free, dissolved, mobile, diffusible) solute concentration (w/v)
B	bound solute concentration (w/v)
K	partition coefficient, or binding equilibrium constant (distinguished by subscript "eq")
k	binding rate constant
Q	unbound solute concentration expressed as a mass ratio (mass solute / mass water)
q	bound solute concentration expressed as a mass ratio (mass solute / mass keratin)
s	bound solute concentration expressed as mass of solute per keratin surface area

Greek letters

α, β	coefficients in property correlations based on octanol/water partition coefficient
γ	empirical scaling factor for binding rate constants
η	binding equilibrium constant based on per-area bound concentration
κ	binding rate constant in rate expression based on per-area bound concentration
λ	ratio of solute to keratin microfibril radii
ρ	density
ϕ	ultrascopic volume fraction within corneocytes
φ	microscopic volume fraction within the SC

Subscripts, superscripts and other affixes

avg	subscript distinguishing average (superficial) concentration representing unbound or bound solute per total (protein + solution) volume in an aqueous dispersion of keratin microfibrils, or per total (corneocyte + lipid) volume in the SC
cor	superscript referring to the corneocyte phase of the SC seen at the microscopic scale
eq	subscript distinguishing binding equilibrium constants
lip	superscript referring to the lipid phase of the SC seen at the microscopic scale
ker	superscript referring to keratin microfibrils seen at the ultrascopic scale
o	superscript referring to octanol
off	subscript distinguishing "off" (unbinding) rate constants
on	subscript distinguishing "on" (binding) rate constants
sc	superscript referring to the SC seen at the macroscopic scale
solute	superscript referring to the solute
true	subscript distinguishing unbound solute concentration based on aqueous solution volume
w	superscript referring to water
no overbar	distinguishes ultrascopic properties (applies to keratin microfibrils)
one overbar	distinguishes microscopic properties (applies to lipid and corneocyte phases of the SC)
two overbars	distinguish macroscopic properties (applies to the SC)

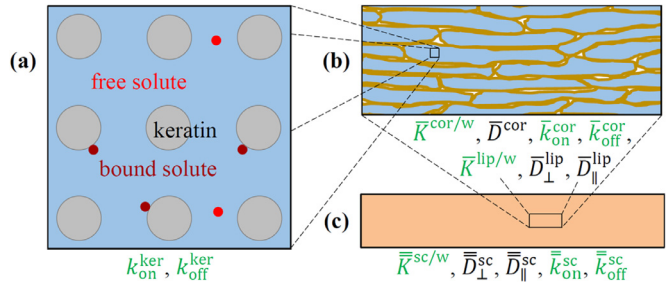

Figure 1. Views of SC tissue at three different scales, progressing from smallest to largest. (a) Ultrastructure of corneocyte interior. (b) Microstructure of SC, with corneocyte and intercellular lipid phases respectively colored blue and yellow. (c) Macrostructure of SC (homogenized effective medium). Green symbols represent parameters of primary importance to our analysis, namely partition and binding rate coefficients characterizing any given solute at the three scales considered. In panel (a) the symbol k_{on}^{ker} is used to represent any of the rate coefficients κ_{on}, $k_{on,q,Q_{true}}$ or $k_{on,q,C_{true}}$, depending on the concentration basis used, with a corresponding understanding for k_{off}^{ker} (see text and Fig. 4 below). The ultrastructure of the lipid phase is not depicted, because there is no solute binding to any constituent of this phase, i.e., binding occurs only within corneocytes. (For interpretation of the references to colour in this figure legend, the reader is referred to the web version of this article.)

"Microscopic" refers to the scale at which the two phases of the SC are discernible[12] (Fig. 1(b)). It comprises ~15 layers of flattened, interleaved, partially desiccated, keratinized cells (corneocytes, "cor") which are embedded in a lipid matrix ("lip") having an ordered (non-liquid-like) molecular structure in a "brick-and-mortar" framework. Figure 1(b) lists the microscopic coefficients describing the two phases seen at this scale, distinguished by a single overbar (−) affix.

"Ultrascopic" refers to the scale at which the substructures of the microscopic phases are discernible (Fig. 1(a)). Of particular interest here is the ultrastructure of the corneocyte phase, which comprises an aqueous dispersion of keratin intermediate filaments called microfibrils, and represents the primary seat of solute binding to the SC, although possible perturbations by cornified cell envelope proteins will also be discussed. The symbols k_{on}^{ker} and k_{off}^{ker} indicated in Figure 1 (a) are shorthand for a number of ultrascopic rate coefficients introduced in our analysis depending on the concentration units used.

For any given solute, the parameters of primary importance to our analysis, namely partition and binding rate coefficients at the three scales considered, are distinguished using green font in Figure 1.

Keratin Structure and Effects of Hydration

SC keratin is classified as an α-keratin and at another level as a soft keratin, distinguishing it from hard α-keratins such as hair, nail and (notably for this study) bovine horn and hoof (BHH). The "α" designation refers to the secondary α-helix structure of the assembled primary filaments, the alternative regular secondary structure being the β-sheets found in feather, beak and claw.[13] Hard and soft keratins are distinguished chemically by the level of crosslinking, which is in turn determined by the amount of sulfur-containing cysteine residues in the primary structure. The soft keratin microfibrils in the SC are oriented predominately in the plane of the tissue, where they are moderately crosslinked.[14] Crosslinking in the transverse direction is minimal, allowing the tissue to swell substantially in this direction when exposed to water.[14,15]

Much is known about the water binding capacity of both hard and soft α-keratins. It has long been argued that dry keratin unfolds as it hydrates, exposing more primary surface area in the process.[16,17] Notably for our analysis, this unfolding process is thought to be largely complete by the time the water content is 20–30 wt% (see Refs. 15 and 18 and references therein). This conclusion is reached by comparing data collected by a variety of techniques. This fact underlies the assumption, implicit in our analysis, that the primary difference between the keratin in partially hydrated (30% w/w water) and fully hydrated

(78% w/w water) skin lies in the microfibril density, rather than the nature of the surfaces exposed at these two levels of hydration.

The precise structure of SC keratin intermediate filaments is not as well characterized as that of wool or hair. For the present analysis we will use the term microfibrils, and regard them as solid cylindrical objects with a characteristic diameter of 7.0 nm[12,13,19] which reversibly bind solute molecules on their surfaces.

Overall State of the Art of SC Transport Modeling and Experimental Characterization

An important use of microscopic diffusion models of the SC lies in producing accurate homogenized partition and transdermal diffusion coefficients $\overline{\overline{K}}^{sc/w}$ and $\overline{\overline{D}}^{sc}_{\perp}$ to be slotted into macroscopic calculators that solve for the transient distribution of solute within the skin for toxicological and other applications.[20–23] The most complete models[24–28] incorporate the strong diffusional anisotropy of the lipid phase, the diffusivity $\overline{\overline{D}}^{lip}_{\parallel}$ for solute motion parallel to the plane of the lipid typically being 2–5 orders of magnitude larger than the diffusivity $\overline{\overline{D}}^{lip}_{\perp}$ for motion perpendicular to it. The latest advance is an extension of the theory to calculate $\overline{\overline{D}}^{sc}_{\parallel}$ in addition to $\overline{\overline{D}}^{sc}_{\perp}$.[27,28] Although a considerable experimental database exists on steady state permeability coefficients and lag times for solute motion through the skin,[29–32] which establishes $\overline{\overline{D}}^{sc}_{\perp}$ for many solutes, comparatively very few determinations of $\overline{\overline{D}}^{sc}_{\parallel}$ have been reported.[33–38] Theory and experiments are in agreement on the finding that — considered as a macroscopic effective continuum — the SC is strongly anisotropic, as the lipid phase is microscopically. Theoretical predictions of the ratio $\overline{\overline{D}}^{sc}_{\parallel}/\overline{\overline{D}}^{sc}_{\perp}$ in the range from 34 to 39 for fully hydrated skin and 150 to more than 1000 for partially hydrated skin[28] accord with the limited available data.

Solute Binding to Keratin During Transport

Promising as it is, the comparison between theory and experiment just noted illustrates an important current stumbling block. Application of even the best microscopic models is presently restricted to two limits: (i) short times (before significant binding has occurred, so that unbound solute is characterized); and (ii) long times (after binding equilibrium has been reached, so that equilibrated total (unbound + bound) solute is characterized). Thus, for example, Wang et al.[28] demonstrate, *inter alia*, the inequalities

$$\begin{array}{lllll} (\overline{\overline{D}}^{sc}_{\parallel})^{calc.}_{free+bound} & < & (\overline{\overline{D}}^{sc}_{\parallel})^{expt.} & < & (\overline{\overline{D}}^{sc}_{\parallel})^{calc.}_{free}, \\ 7.25\times10^{-10} & < & 3.7\times10^{-9} & < & 7.87\times10^{-9} \quad cm^2/s \text{ for solute caffeine,} \\ 3.25\times10^{-9} & < & 7.8\times10^{-9} & < & 8.47\times10^{-9} \quad cm^2/s \text{ for solute testosterone,} \end{array} \tag{1}$$

where the numerical values given here apply to partially hydrated skin. The short- and long-time limits calculated from a microscopic model successfully bracket the more complicated transient in real dermal absorption scenarios, which start with all unbound solute, and end with equilibrium bound solute, but the match is limited to such inequalities. Thus, prediction of actual absorption transients is not yet possible.

A few papers have established the value of adding reversible binding to diffusion models of transient dermal absorption.[7,9] This step is taken by introducing a bound (immobile) solute concentration field $\overline{\overline{B}}^{sc}$ which coevolves with the unbound (mobile) solute concentration $\overline{\overline{C}}^{sc}$. Unfortunately, this approach has only been brought to fruition at the macroscopic scale to date, so that effective "on" and "off" binding rate constants $\overline{\overline{k}}^{sc}_{on}$ and $\overline{\overline{k}}^{sc}_{off}$ have been determined only from best fits to permeation and/or desorption transients.

As represented by the gray arrow in Figure 2, Nitsche and Frasch[8] have worked out the micro-macro link (homogenization) for linear reversible binding, and shown how $\overline{\overline{k}}^{sc}_{on}$ and $\overline{\overline{k}}^{sc}_{off}$ (see Fig. 1(c)) can be calculated from the microscopic corneocyte-phase rate constants $\overline{k}^{cor}_{on}$ and $\overline{k}^{cor}_{off}$ (see Fig. 1(b)). Thus, all the requisite pieces are in place to assemble, at least in principle, the next generation of microscopic models capable of fully predicting dermal absorption transients. The conceptual missing link needed to do so, represented by the upper blue arrow in Figure 2, is the relationship of $\overline{k}^{cor}_{on}$ and $\overline{k}^{cor}_{off}$ to the ultrascopic rate constants k^{ker}_{on} and k^{ker}_{off} quantified by keratin binding studies. The present paper establishes this link.

Keratin Binding Studies

Fundamental keratin binding studies define binding at the ultrascopic scale at which individual keratin microfibrils are discernible. For various types of keratin, numerous studies have established the

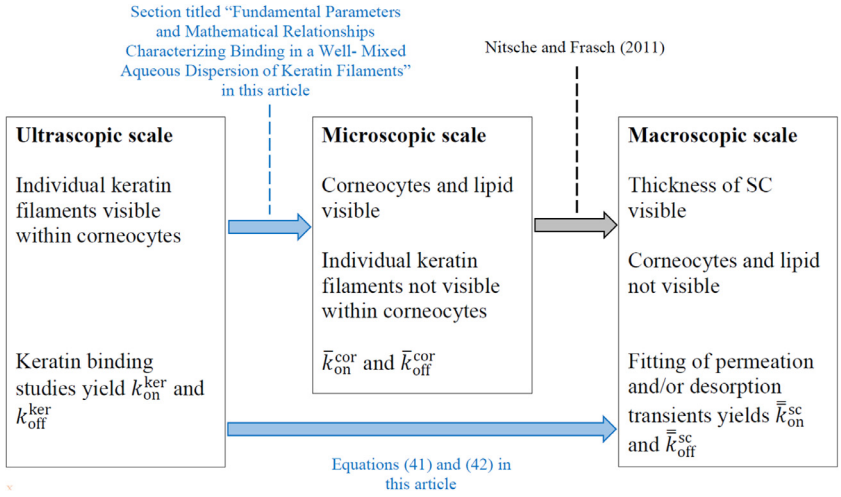

Figure 2. Scheme indicating the role of the present analysis vis-à-vis previously published work (Nitsche and Frasch (2011)[8]) in connecting ultrascopic, microscopic and macroscopic descriptions of solute–keratin binding in the SC. Desorption experiments with delipidized SC could shed light on $\overline{k}^{cor}_{on}$ and $\overline{k}^{cor}_{off}$.

dilute-limit equilibrium relationship $q = K_{\text{Nernst}} C_{\text{true}} = (k_{\text{on}}^{\text{ker}}/k_{\text{off}}^{\text{ker}}) C_{\text{true}}$ between bound solute loading q (mg solute/g protein) and unbound solute concentration C_{true}, as analyzed comprehensively across a broad spectrum of solutes by Hansen et al. (2011).[39] Values of $\log_{10} K_{\text{Nernst}}$ for bovine horn and hoof (BHH) keratin tend to be consistently higher than for delipidized SC and callus keratin by ~ 0.6 $\log_{10}$ units (factor of ~ 4), and both correlate with the logarithm of the octanol/water distribution coefficient ($\log_{10} D^{\text{o/w}}$, measure of solute lipophilicity) with slopes around 0.3. Thus, a basis exists to estimate binding equilibrium constants for the SC keratin of interest.

Additionally, Seif and Hansen[10] have measured eight values of $k_{\text{off}}^{\text{ker}}$ (and by inference $k_{\text{on}}^{\text{ker}} = K_{\text{Nernst}} k_{\text{off}}^{\text{ker}}$) for six solutes with BHH keratin, i.e., the kinetics of the binding process. Their study suggests an intriguing correlation between $k_{\text{off}}^{\text{ker}}$ and K_{Nernst} for BHH keratin, which in principle opens the possibility of predicting $k_{\text{off}}^{\text{ker}}$.

Role and Structure of the Present Analysis

The experimental kinetic study reported by Seif and Hansen,[10] and the correlations suggested by it, are highly significant. The choice of solutes addressed is propitious and well considered, covering as it does a wide range of lipophilicities ($-0.13 \leq \log_{10} D^{\text{o/w}} \leq 3.80$). (Seif and Hansen use the symbol K_{pH} for the octanol/water distribution coefficient $D^{\text{o/w}}$, apparently to underscore the fact that it is measured at a certain pH.) Nevertheless, the fact that available data are currently limited to just six solutes underscores the great importance of further kinetic measurements to broaden the physicochemical spectrum considered. The need for such work, as well as comparisons between rate constants measured for BHH vis-à-vis delipidized human SC and callus keratin, cannot be filled by theoretical analysis. Thus, substantially fuller resolution of transient solute–keratin binding as it occurs in human dermal absorption scenarios must await completion of a significant body of experiments.

The specific purpose of this analysis is to develop the quantitative framework needed to understand, utilize and unify the results of keratin binding studies carried out with different types of keratin, with a view toward ultimately parameterizing dermal absorption models that explicitly address the interplay between solute diffusion and binding, and thereby realistically represent the transients characterizing these combined and coevolving processes. Not least among the benefits of such a framework is the ability it confers to quantify the dependence of the effective (homogenized, coarse-grained) "on" (binding) and "off" (unbinding) rate constants $\overline{\overline{k}}_{\text{on}}^{\text{sc}}$ and $\overline{\overline{k}}_{\text{off}}^{\text{sc}}$ on the hydration state of the SC, permitting measurements with fully hydrated SC to be translated into outcomes involving partially hydrated SC. To this end, a preliminary theoretical section establishes fundamental parameters and mathematical relationships characterizing binding in keratin dispersions. Successive sections below then summarize theoretical methodology and results entering the analysis, and work out the propagation of kinetic information from ultrascopic to macroscopic scales, leading to a useful set of formulas collected and commented upon in Results and Discussion sections.

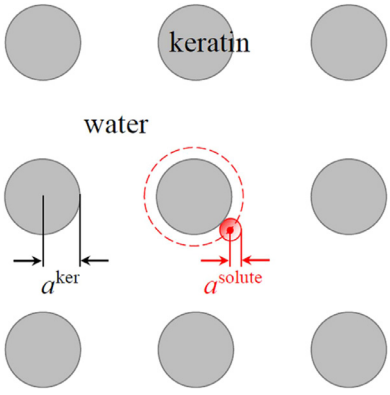

Figure 3. Simplified conceptualization of a dispersion of keratin microfibrils in water as seen in cross section. Steric (geometric) exclusion of solute centers from an annular layer of thickness a^{solute} around each keratin microfibril is represented by a red dashed circle around one of the microfibrils. (For interpretation of the references to colour in this figure legend, the reader is referred to the web version of this article.)

A significant part of the analysis involves the establishment of connections among different concentration units used in keratin binding and dermal absorption studies at the three scales considered. Certain aspects of the analysis are partly speculative, and speculative elements are clearly identified as such. The entire development refers to the intrinsic properties of defect-free interappendageal SC, ultimately considered as a homogenized continuum. Thus, possible impact of appendages such as hair follicles in presenting binding sites and a macroporous polar pathway through the SC lie outside the scope of our analysis. However, the results developed could be incorporated into a broader macroscopic model of the SC that includes appendages.

Fundamental Parameters and Mathematical Relationships Characterizing Binding in a Well-Mixed Aqueous Dispersion of Keratin Microfibrils

Equations are developed describing solute–keratin binding equilibria and kinetics. They characterize a well-mixed aqueous dispersion of keratin microfibrils in a keratin binding study, and are later applied to the microscopic corneocyte phase of the SC considered at the ultrascopic scale at which individual keratin microfibrils are discernible.

No assumption is made about the arrangement of microfibrils aside from the stipulation that they are mostly separated from each other and therefore do not substantially block binding sites on each other's surfaces, i.e., act as independent 'sticky' surfaces. This stipulation would require modification for a dense (tightly-packed) dispersion. As a convenient visual conceptualization, the dispersion might be imagined as a square array of parallel microfibrils as shown in Figure 3, although no such assumption about the arrangement of microfibrils enters the following analysis.

Structure

The key structural parameters are the microfibril radius a^{ker} (~ 3.5 nm for human SC[12,19] and α-keratin generally[13]) and volume fraction ϕ^{ker}. In terms of them, the mass of keratin m^{ker} in a given total volume of the dispersion V^{total}, and the aggregated total (lateral, cylindrical) surface area of this protein S^{ker}, are given by the equations

$$m^{\text{ker}}/V^{\text{total}} = \phi^{\text{ker}} \rho^{\text{ker}}, \tag{2}$$

$$S^{\text{ker}}/m^{\text{ker}} = 2/(\rho^{\text{ker}} a^{\text{ker}}), \tag{3}$$

where ρ^{ker} denotes the protein density (≈ 1.37 g/cm^3).[40–43] The inverse (reciprocal) dependence of surface area upon a^{ker} in Eq. (3) embodies the fact that — for any given type of shape, here cylindrical — the smaller the particles of a solid material are the more surface area a given mass of them presents collectively.

Unbound Solute Concentration

The symbols C_{true} (g solute/cm^3 aqueous volume) and Q_{true} (g solute/g water) are respectively taken to denote w/v and mass ratio concentrations of a given solute in the aqueous volume encompassing one (or more) keratinous objects. They are related by the expression

$$C_{\text{true}} = Q_{\text{true}} \rho^{\text{w}} \times \underbrace{\left(\frac{\text{cm}^3 \text{ water}}{\text{cm}^3 \text{ solution}} \right)}_{[\text{v.c.}]}, \tag{4}$$

in which ρ^{w} denotes the density of water ($\cong$ 1 g/cm^3) and "[v.c.]" is introduced as shorthand for the volume correction exhibited within the large parentheses. Although the factor "[v.c.]" is included in several equations below as needed for technical correctness, its numerical value can be regarded as practically indistinguishable from unity for the low concentrations assumed here.

It is also useful to consider an average (superficial) concentration representing the amount of unbound solute per total volume of the dispersion of keratin microfibrils. Such a concentration is here called C_{ave} (g unbound solute/cm^3 keratin dispersion). The descriptor "total" encompasses both the aqueous domain between the microfibrils, and the impenetrable microfibrils themselves. The average is computed as the concentration C_{true} multiplied by the volume fraction $1-\phi^{ker}(1+\lambda)^2$ accessible to solute centers, which yields

$$C_{avg} = \left[1-\phi^{ker}(1+\lambda)^2\right] C_{true}, \tag{5}$$

in which

$$\lambda = a^{solute}/a^{ker} = a^{solute}/(35\ \text{Å}) \tag{6}$$

denotes the ratio of solute to keratin microfibril radii. Equation (5) includes the effects of steric (geometric) exclusion of solute centers from an annular layer of thickness a^{solute} around each keratin microfibril, represented by a red dashed circle around one of the microfibrils depicted in Figure 3 (see Wang et al.'s[25] Eq. (11) and surrounding text).

Bound Solute Concentration

In experiments the bound (immobile) amount of a given solute is commonly quantified per mass of keratin using a concentration variable q (g solute/g keratin).[10,39] In certain applications an average concentration representing the amount of bound solute per total volume of the dispersion of keratin microfibrils is also useful to consider. Such a concentration is here called B_{avg} (g bound solute/cm^3 keratin dispersion). Ultimately the most fundamental quantification of bound solute would appear to be per keratin surface area using a concentration variable here named s (g solute/cm^2 keratin surface area). Indeed, one can imagine that a keratinous object of cylindrical (or any other) shape would tend to bind a definite number of solute molecules per area if equilibrated with a surrounding solution of a given concentration C_{true}. The reason is that binding occurs as a surface phenomenon (as opposed to, say, a process distributed throughout the volume of the protein, which is unlikely because the microfibrils are very dense). Using Eqs. (2) and (3), the three bound concentration variables discussed can be shown to be related by the equations

$$q = (S^{ker}/m^{ker})s = \left[2/(\rho^{ker}a^{ker})\right]s, \tag{7}$$

$$B_{avg} = \left(m^{ker}/V^{total}\right)q = \rho^{ker}\phi^{ker}\,q = \left(2\phi^{ker}/a^{ker}\right)s. \tag{8}$$

Binding Equilibrium

At low solute concentrations the most fundamental binding equilibrium relationship would appear to be a proportionality between the bound surface concentration s and the surrounding aqueous-phase concentration C_{true}:

$$s = \eta\, C_{true}. \tag{9}$$

The bound and unbound solute concentration units used make η a binding equilibrium constant with the dimensions of length. This most fundamental relationship can be converted into mathematically equivalent relationships alternately involving q or B_{avg} on the left-hand side, and C_{true}, Q_{true} or C_{ave} on the right-hand side. Thus, for instance, Eq. (9) leads to the relationships

$$q = \underbrace{\left(\frac{2\eta}{\rho^{ker}a^{ker}}\right)}_{K_{eq,q,C_{true}}} C_{true}, \tag{10}$$

$$q = \underbrace{\left(\frac{2\eta\rho^{w}[\text{v.c.}]}{\rho^{ker}a^{ker}}\right)}_{K_{eq,q,Q_{true}}} Q_{true}, \tag{11}$$

$$B_{avg} = \underbrace{\left[\frac{2\eta}{a^{ker}}\cdot\frac{\phi^{ker}}{1-\phi^{ker}(1+\lambda)^2}\right]}_{K_{eq,B_{avg},C_{avg}}} C_{avg}. \tag{12}$$

The symbols below the underbraces in these equations define equilibrium constants appropriate for the types of concentration variables used. The group labeled as $K_{eq,q,C_{true}}$ in Eq. (10) is equivalent to Hansen et al.'s[39] Nernst binding coefficient K_{Nernst} defined by their Eq. (4). The group labeled as $K_{eq,q,Q_{true}}$ in Eq. (11) is equivalent to Seif and Hansen's[10] coefficient K_b defined by their Eq. (2), and to Raykar, Anderson et al.'s[44,45] partition coefficient PC_{pro} (used by them and other authors[43,46,47] with slight notational variations in the context of SC keratin). Notation indicating the type of bound concentration (q or B_{avg}) and unbound concentration (C_{true}, Q_{true} or C_{ave}) entering the definition of a binding equilibrium constant K_{eq} is necessarily complex. Figure 4 details how symbols representing these types of concentrations are appended to the subscript "eq" to disambiguate the symbol K_{eq}. Final results are ultimately cast in terms equilibrium (and also binding rate) constants based on the bound concentration q and the unbound concentration Q_{true}, and abbreviated as $K_{eq}^{ker} \equiv K_{eq,q,Q_{true}}$, etc.

Although equilibrium binding data are often reported in terms of the unbound and bound concentrations C_{true} and q, and fitted using Eq. (10),[39] Eq. (9) expressed per keratin surface area represents the most fundamental quantitative statement of linear reversible binding equilibrium.

Binding Kinetics

The binding rate expression consistent with Eq. (9) is

$$ds/dt = \kappa_{on}\, C_{true} - \kappa_{off}\, s, \tag{13}$$

in which rate constants κ_{on} and κ_{off} have dimensions of velocity and reciprocal time, respectively. At equilibrium $ds/dt = 0$, which makes

$$s = (\kappa_{on}/\kappa_{off})C_{true}. \tag{14}$$

Comparison with Eq. (9) yields the expected relationship

$$\eta = \kappa_{on}/\kappa_{off}. \tag{15}$$

Based on preceding relationships between different types of unbound and bound solute concentrations, the most fundamental rate expression expressed per keratin surface area by Eq. (13) implies the mathematically equivalent rate expressions

$$\frac{dq}{dt} = \underbrace{\left(\frac{2\,\kappa_{on}}{\rho^{ker}a^{ker}}\right)}_{k_{on,q,C_{true}}} C_{true} - \underbrace{\kappa_{off}}_{k_{off,q,C_{true}}}\, q, \tag{16}$$

$$\frac{dq}{dt} = \underbrace{\left(\frac{2\,\kappa_{on}\rho^{w}[\text{v.c.}]}{\rho^{ker}a^{ker}}\right)}_{k_{on,q,Q_{true}}} Q_{true} - \underbrace{\kappa_{off}}_{k_{off,q,Q_{true}}}\, q, \tag{17}$$

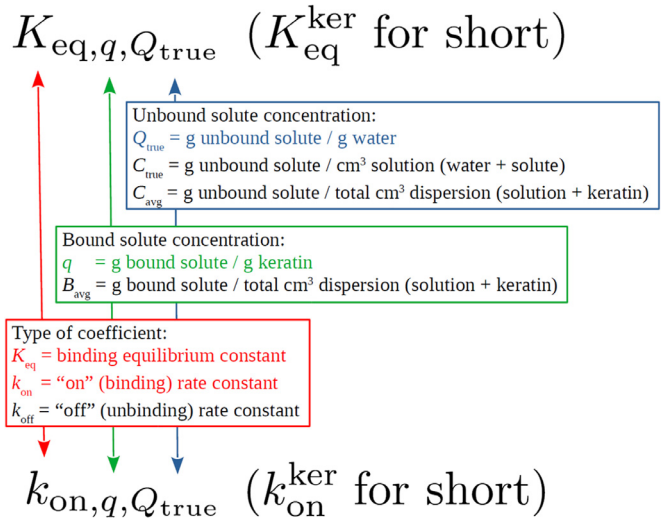

Figure 4. Scheme explaining the notation used to disambiguate the symbols K_{eq}, k_{on} and k_{off} for binding equilibrium constants, "on" (binding) rate constants and "off" (unbinding) rate constants, respectively.

$$-\frac{dC_{\mathrm{avg}}}{dt}=\frac{dB_{\mathrm{avg}}}{dt}=\underbrace{\left[\frac{2\,\kappa_{\mathrm{on}}}{a^{\mathrm{ker}}}\cdot\frac{\phi^{\mathrm{ker}}}{1-\phi^{\mathrm{ker}}(1+\lambda)^2}\right]}_{k_{\mathrm{on},B_{\mathrm{avg}},C_{\mathrm{avg}}}}C_{\mathrm{avg}}-\underbrace{\kappa_{\mathrm{off}}}_{k_{\mathrm{off},B_{\mathrm{avg}},C_{\mathrm{avg}}}}B_{\mathrm{avg}}. \tag{18}$$

The symbols below the underbraces in these equations define "on" (binding) and "off" (unbinding) rate constants appropriate for each type of concentration variable used, following the notational scheme introduced for binding equilibrium constants (see Fig. 4). Analogously to Eq. (15), the expected relationships

$$K_{\mathrm{eq},q,Q_{\mathrm{true}}}=k_{\mathrm{on},q,Q_{\mathrm{true}}}/k_{\mathrm{off},q,Q_{\mathrm{true}}}, \tag{19}$$

$$K_{\mathrm{eq},B_{\mathrm{avg}},C_{\mathrm{avg}}}=k_{\mathrm{on},B_{\mathrm{avg}},C_{\mathrm{avg}}}/k_{\mathrm{off},B_{\mathrm{avg}},C_{\mathrm{avg}}} \tag{20}$$

utilized below can be verified by setting $dq/dt=0$ in Eq. (17) and comparing the relation that results with Eq. (11), and by setting $dB_{\mathrm{avg}}/dt=0$ in Eq. (18) and comparing the relation that results with Eq. (12), respectively.

Use of Keratin Binding Data

Preceding equations make it possible to convert binding parameters determined on one concentration basis to be translated into another concentration basis. Thus, for instance, determinations of $K_{\mathrm{eq},q,Q_{\mathrm{true}}}$ and $k_{\mathrm{off},q,Q_{\mathrm{true}}}$ (basis of q and Q_{true}; cf. Hansen et al.[48] and Seif and Hansen[10]) could be used to establish the values of $K_{\mathrm{eq},B_{\mathrm{avg}},C_{\mathrm{avg}}}$ and $k_{\mathrm{off},B_{\mathrm{avg}},C_{\mathrm{avg}}}$ (basis of B_{avg} and C_{avg}) via the relationships

$$K_{\mathrm{eq},B_{\mathrm{avg}},C_{\mathrm{avg}}}=\frac{\rho^{\mathrm{ker}}}{\rho^{\mathrm{w}}[\mathrm{v.c.}]}\cdot\frac{\phi^{\mathrm{ker}}}{1-\phi^{\mathrm{ker}}(1+\lambda)^2}\cdot K_{\mathrm{eq},q,Q_{\mathrm{true}}}, \tag{21}$$

$$k_{\mathrm{off},B_{\mathrm{avg}},C_{\mathrm{avg}}}=k_{\mathrm{off},q,Q_{\mathrm{true}}}. \tag{22}$$

A separate equation for $k_{\mathrm{on},B_{\mathrm{avg}},C_{\mathrm{avg}}}$ is not needed, because this coefficient follows immediately from Eq. (20).

Simplified Notation

At this point it is worthwhile to adopt a default convention of always using average (superficial) concentrations, and — with this practice understood — dropping the subscripts "avg" on concentrations, and "$B_{\mathrm{avg}}, C_{\mathrm{avg}}$" on binding equilibrium and rate constants, for notational simplicity. The reason is that the concentration basis underlying the diffusion equation formulated at all scales is average (superficial) per-volume concentration. Therefore, from now on we make the following notational simplifications:

$$\begin{aligned} C_{\mathrm{avg}} &\Rightarrow \overline{C},\\ B_{\mathrm{avg}} &\Rightarrow \overline{B},\\ K_{\mathrm{eq},B_{\mathrm{avg}},C_{\mathrm{avg}}} &\Rightarrow \overline{K}_{\mathrm{eq}},\\ k_{\mathrm{on},B_{\mathrm{avg}},C_{\mathrm{avg}}} &\Rightarrow \overline{k}_{\mathrm{on}},\\ k_{\mathrm{off},B_{\mathrm{avg}},C_{\mathrm{avg}}} &\Rightarrow \overline{k}_{\mathrm{off}}. \end{aligned} \tag{23}$$

The overbars serve as a reminder of the fact that all symbols represent volume-average attributes of the aqueous dispersion of keratin microfibrils.

Methods

Octanol/Water Partition Coefficients

Following subsections present correlations giving binding equilibrium and rate constants arising in preceding equations, as well as a partition coefficient also needed below, as functions of $\log_{10}$ of the octanol/water partition coefficient of the solute ($\log_{10}K^{\mathrm{o/w}}$, measure of lipophilicity). Numerical values of $\log_{10}K^{\mathrm{o/w}}$ for three solutes considered below as examples (theophylline, testosterone, water) are obtained from the Estimation Program Interface (EPI) Suite, U.S. Environmental Protection Agency[49] accessed through ChemSpider.[50] An experimental database match is indicated for all three.

Estimation of Partition Coefficients of Microscopic Lipid and Corneocyte Phases

Numerous authors[39,43,46,47,51,52] have presented correlations of the form

$$\log_{10}\overline{k}^{\mathrm{lip/w}}=\alpha^{\mathrm{lip}}+\beta^{\mathrm{lip}}\log_{10}K^{\mathrm{o/w}} \tag{24}$$

(with variations in notation) approximately characterizing the lipophilicity dependence of the SC lipid/water partition coefficient. Table 1 lists published best-fit values of the constants α^{lip} and β^{lip} resulting from these analyses of various datasets. Following standard convention, the symbol "K" is used to denote partition coefficients representing ratios of w/v (per-volume) concentrations in the two phases being compared. Some of the cited authors[44–47] report partition coefficients "PC" representing ratios of mass ratio concentrations. They are converted to "K" using Nitsche and Kasting's[52] Eq. (2), namely

$$\overline{K}^{\mathrm{lip/w}}=0.937\,\mathrm{PC}^{\mathrm{lip/w}}. \tag{25}$$

For illustrative purposes we utilize the latest iterate[52]

$$\log_{10}\overline{K}^{\mathrm{lip/w}}=0.12+0.67\,\log_{10}K^{\mathrm{o/w}} \tag{26}$$

Table 1
Constants Appearing in Published Correlations Having the Forms of Eqs. (24) and (30) Giving ($\log_{10}$ of the) SC Lipid/Water Partition Coefficient $\log_{10}\overline{K}^{\mathrm{lip/w}}$ and Keratin Binding Equilibrium Constant $\log_{10}K_{\mathrm{eq},q,Q_{\mathrm{true}}}$ as Functions of $\log_{10}K^{\mathrm{o/w}}$.

Analysis	α^{lip}	β^{lip}	α^{cor}	β^{cor}
Raykar et al. (1988)[44]	−0.85[a]	0.91[a]	0.87	0.24
Anderson and Raykar (1989)[45]			0.75	0.27
Mitragotri (2002)[51]	0	0.7		
Nitsche et al. (2006)[43]	−0.37	0.81	0.73	0.27
Wang et al. (2010)[46]	0.19[a]	0.62[a]	0.62	0.31
Hansen et al. (2011)[39][b]			0.65	0.32
Hansen et al. (2013)[47]	0.092[a]	0.67[a]	**0.73**	**0.32**
Nitsche and Kasting (2018)[52]	**0.12**	**0.67**		

Boldface type distinguishes values selected to make estimates in this analysis.
[a] $\mathrm{PC}_{\mathrm{lip/w}}$ is converted to $\overline{K}^{\mathrm{lip/w}}$ using Eq. (25).
[b] Stated values represent the authors' "Unified" ("BHH-corr. ± CAL ± DSC") fit.

based on the most comprehensive dataset analyzed to date, which differs little from earlier formulas proposed by Mitragotri[51] and Hansen et al.[47] The fit is over the range $0 \lesssim \log_{10}K^{o/w} \lesssim 5.5$, and specifically excludes a datum for water. None of the published correlations can be considered reliable for hydrophilic solutes.

The corneocyte/water partition coefficient $\overline{K}^{cor/w}$ is understood here to characterize only unbound solute. As discussed early on by Raykar et al.[44] this coefficient represents solute dissolution in the water that hydrates corneocytes. It is determined by the fraction of the volume occupied (and thereby rendered inaccessible) by keratin, with additional steric exclusion owing to the nonzero radius of the solute molecule noted in connection with Eq. (5) above. According to Nitsche et al.'s[43] volumetric bookkeeping,

$$\overline{K}^{cor/w} = 1 - \phi^{ker}(1+\lambda)^2 = \begin{cases} 1 - 0.1928\,(1+\lambda)^2 & \text{(fully hydrated)} \\ 1 - 0.6044\,(1+\lambda)^2 & \text{(partially hydrated)}, \end{cases} \tag{27}$$

which indicates dependence on the hydration state of the SC (see Wang et al.'s[25] Eqs. (11) and (12), and corresponding equations in their Tables 3 and 4). This formula is synonymous with the factor in square brackets in Eq. (5) because of the definition of $\overline{K}^{cor/w}$, which represents the ratio of the average solute concentration in the corneocyte phase to the solute concentration in an adjacent aqueous solution at equilibrium. This ratio is precisely C_{avg}/C_{true} in the parlance of Eq. (5), because water within corneocytes has the same solvent properties as bulk water.[44] The solute radius needed to compute λ (see Eq. (6)) is given by the equation

$$\begin{aligned} a^{solute} &= \text{Stokes–Einstein equivalent radius of solute} \\ &= \begin{cases} (0.145\ \text{Å})(V_A)^{0.6} & \text{if } V_A \le 445.2, \\ (0.735\ \text{Å})(V_A)^{1/3} & \text{if } V_A > 445.2 \end{cases} \end{aligned} \tag{28}$$

according to Wang et al.[25] Here V_A denotes the solute molar volume as a liquid at its normal boiling point in units of cm^3/mol, estimated using Schroeder's method (see Wang et al.'s Eq. (B3) and following text, or Poling et al.'s[53] Eq. (4-10.1) on their p. 4.33). We note for completeness that a distinct partition coefficient quantifying equilibrium uptake of all (unbound + bound) solute would be given by[7,9]

$$(\overline{K}^{cor/w})_{unbound+bound} = \overline{K}^{cor/w}\left(1 + \overline{k}^{cor}_{on}/\overline{k}^{cor}_{off}\right). \tag{29}$$

This latter partition coefficient is not a directly useful parameter in calculations that seek to resolve permeation transients as influenced by keratin binding kinetics, discussed in the Introduction.

Estimation of Ultrascopic Binding Equilibrium Constant

Table 1 includes published values of the constants α^{cor} and β^{cor} appearing in published correlations of the form

$$\log_{10}K_{eq,q,Q_{true}} = \alpha^{cor} + \beta^{cor}\log_{10}K^{o/w} \tag{30}$$

approximately characterizing the lipophilicity dependence of the binding equilibrium constant $K_{eq,q,Q_{true}}$. The superscript "cor" affixed to the constants reflects the fact that they derive wholly or partly from fits of data measured with delipidized human SC. The meaning of our symbol $K_{eq,q,Q_{true}}$ is synonymous with that of Seif and Hansen's[10] symbol K_b and Raykar, Anderson et al.'s[44,45] symbol PC_{pro} (used by them and other authors[43,46,47] with slight notational variations). Its numerical value is practically indistinguishable from that of $K_{eq,q,C_{true}}$ (called K_{Nernst} by Hansen et al.[39]) owing to the relation

$$K_{eq,q,C_{true}} = \frac{K_{eq,q,Q_{true}}}{\rho^w[\text{v.c.}]} \tag{31}$$

(which derives from Eqs. (10) and (11)) together with the fact that $\rho^w \cong 1$ g/cm^3 and [v.c.] $\cong 1$. Thus all the constants α^{cor} and β^{cor} listed in Table 1 effectively characterize the dependence of $\log_{10}K_{eq,q,Q_{true}}$ (or $\log_{10}K_{eq,q,C_{true}}$) on $\log_{10}K^{o/w}$.

None of the fits represented in Table 1 differs substantively from Raykar, Anderson et al.'s pioneering and prescient original analysis,[44,45] so there is not much to choose between them. We settle on Hansen et al.'s[47] formula

$$\log_{10}K_{eq,q,Q_{true}} = 0.73 + 0.32\,\log_{10}K^{o/w} \tag{32}$$

for illustrative calculations below for two reasons. First, it is based on the most comprehensive equilibrium binding dataset analyzed to date. Second, the fitting incorporates a significant and useful finding emerging from Hansen et al.'s earlier analysis,[39] namely that $K_{eq,q,Q_{true}}$ for bovine horn and hoof keratin exhibits essentially the same lipophilicity dependence (β^{cor}) as that for human delipidized SC and callus, but is consistently larger by ~ 0.6 $\log_{10}$ units (i.e., a factor of about $10^{0.6} \cong 4.0$). In equation form,

$$\log_{10}(K_{eq,q,Q_{true}})_{BHH} \cong 0.6 + \log_{10}K_{eq,q,Q_{true}}, \tag{33}$$

in which bovine horn and hoof keratin is distinguished with the subscript "BHH."

Estimation of Ultrascopic "Off" (Unbinding) Rate Constant

To our knowledge, direct measurements of binding rate constants do not exist for human SC keratin (as either delipidized SC or callus). For bovine horn and hoof keratin, Seif and Hansen[10] observe a strong correlation between measured values of their rate constant k_{off} and the binding equilibrium constant ($r^2 = 0.994$) based on eight data points for six solutes with $-0.13 \le \log_{10}D^{o/w} \le 3.80$. Some ambiguity arises because both w/v (per-volume) and mass ratio concentrations appear in various of their equations. Whether their symbol k_{off} represents the formal equivalent of $(k_{off,q,Q_{true}})_{BHH}$ or $(k_{off,q,C_{true}})_{BHH}$ is a moot point, however, because these two parameters are identical (cf. Eqs. (16) and (17)). In present notation their best-fit correlation is expressible as

$$\frac{(k_{off,q,Q_{true}})_{BHH}}{\text{min}^{-1}} = \left[25.75 + 0.459\,(K_{eq,q,Q_{true}})_{BHH}\right]^{-1} \tag{34}$$

(cf. their Eq. (10)). As commented by Seif and Hansen, "solutes exhibiting higher $[(K_{eq,q,Q_{true}})_{BHH}]$ at the same time will have smaller $[(k_{off,q,Q_{true}})_{BHH}]$ (or adsorb to a greater extent and take longer to desorb)."

Seif and Hansen also present an equation giving $(k_{off,q,Q_{true}})_{BHH}$ in terms of the octanol/water distribution coefficient, namely

$$\frac{(k_{off,q,Q_{true}})_{BHH}}{\text{min}^{-1}} = \left[25.75 + 8.35\,(K^{o/w})^{0.34}\right]^{-1} \tag{35}$$

in present notation (cf. their Eq. (11)), although the correlation is not as good.

Ultra-to-Micro Homogenization of Binding Kinetics

Eqs. (20)–(22) are used to obtain the microscopic corneocyte-phase properties (with an overbar) from the ultrascopic properties (with no affix) measurable at least in principle via keratin binding studies. In terms of the simplified notation defined by Eq. (23), and with the superscript "cor" signifying application of the theory to the microscopic corneoctye phase, these equations may be cast in the form

$$\overline{k}^{cor}_{on} = \underbrace{\left[\frac{\rho^{ker}}{\rho^w[\text{v.c.}]} \cdot \frac{\phi^{ker}}{1 - \phi^{ker}(1+\lambda)^2}\right]}_{f_{ultra\to micro}} k_{on,q,Q_{true}}, \tag{36}$$

$$\overline{k}_{\mathrm{off}}^{\mathrm{cor}} = k_{\mathrm{off},q,Q_{\mathrm{true}}}. \tag{37}$$

Here ϕ^{ker} represents the volume fraction of keratin microfibrils within corneocytes, the value of which is ~0.19 and ~0.60 in fully and partially hydrated SC, respectively.[43] If needed, the microscopic corneocyte-phase binding equilibrium constant can be determined by taking the ratio of Eqs. (36) and (37) (cf. Eq. (20)).

The derivation of these equations, presented in the preceding section, is based on the assumption that the solute is well mixed throughout the aqueous medium between keratin microfibrils. This condition is likely to be satisfied in keratin binding studies due to intentional stirring. Given the slowness of the binding process and the small (ultrascopic) distances over which dissolved solutes need to diffuse to reach the surfaces of keratin microfibrils, the effect of diffusional resistance on binding kinetics within corneocytes is also likely to be small.

Micro-to-Macro Homogenization of Binding Kinetics

With cosmetic changes to suit the present notation, Nitsche and Frasch's[8] Eq. (59a,b), namely

$$\overline{\overline{k}}_{\mathrm{on}}^{\mathrm{sc}} = \underbrace{\left(\frac{\overline{\varphi}^{\mathrm{cor}}\overline{K}^{\mathrm{cor/w}}}{\overline{\varphi}^{\mathrm{lip}}\overline{K}^{\mathrm{lip/w}} + \overline{\varphi}^{\mathrm{cor}}\overline{K}^{\mathrm{cor/w}}}\right)}_{f_{\mathrm{micro}\to\mathrm{macro}}} \overline{k}_{\mathrm{on}}^{\mathrm{cor}}, \tag{38}$$

$$\overline{\overline{k}}_{\mathrm{off}}^{\mathrm{sc}} = \overline{k}_{\mathrm{off}}^{\mathrm{cor}}, \tag{39}$$

are used to obtain the macroscopic rate constants (with a double overbar) from the microscopic rate constants (with a single overbar). Here $\overline{\varphi}^{\mathrm{lip}}$ and $\overline{\varphi}^{\mathrm{cor}} = 1 - \overline{\varphi}^{\mathrm{lip}}$ denote the volume fractions of the microscopic lipid and corneocyte phases, respectively. The value of $\overline{\varphi}^{\mathrm{lip}}$ is ~0.032 and ~0.093 for fully and partially hydrated SC, respectively.[43] If needed, the macroscopic binding equilibrium constant can be determined by taking the ratio of Eqs. (38) and (39).

Ultra-to-Macro Homogenization of Binding Kinetics

The link between binding rate constants at ultrascopic and macroscopic scales is achieved by sequential application of Eqs. (36) and (37), and then Eqs. (38) and (39).

Results

Rate Constants for Linear Reversible Binding

The outcome of the two-step up-scaling from ultrascopic to macroscopic scales just described is the following pair of formulas giving the effective macroscopic "on" (binding) and "off" (unbinding) rate constants in terms of their ultrascopic counterparts:

$$\overline{\overline{k}}_{\mathrm{on}}^{\mathrm{sc}} = \underbrace{\left[\frac{\overline{\varphi}^{\mathrm{cor}}\overline{K}^{\mathrm{cor/w}}}{\overline{\varphi}^{\mathrm{lip}}\overline{K}^{\mathrm{lip/w}} + \overline{\varphi}^{\mathrm{cor}}\overline{K}^{\mathrm{cor/w}}} \cdot \frac{\rho^{\mathrm{ker}}}{\rho^{\mathrm{w}}[\mathrm{v.c.}]} \cdot \frac{\phi^{\mathrm{ker}}}{1-\phi^{\mathrm{ker}}(1+\lambda)^2}\right]}_{f_{\mathrm{micro}\to\mathrm{macro}}\times f_{\mathrm{ultra}\to\mathrm{micro}}} k_{\mathrm{on},q,Q_{\mathrm{true}}}, \tag{40}$$

$$\overline{\overline{k}}_{\mathrm{off}}^{\mathrm{sc}} = k_{\mathrm{off},q,Q_{\mathrm{true}}}. \tag{41}$$

These equations provide the link between the observable (volume-average) rate constants which would enter the SC diffusion component of a dermal absorption calculator that explicitly represents transient binding, and the keratin mass–based rate constants that would be measured in an in vitro keratin binding study.

Table 2
Properties of the SC in Fully and Partially Hydrated States Entering Eq. (42), Drawn From Nitsche et al.'s[43] Table 1 With Slight Changes in Notation.

Property	Value in fully hydrated state	Value in partially hydrated state
ρ^{w}	1.0 g/cm^3	
ρ^{ker}	1.37 g/cm^3	
[v.c.]	1 (approximation for dilute solutions)	
ϕ^{ker}	0.1928	0.6044
$\overline{\varphi}^{\mathrm{lip}}$	0.0316	0.0927
$\overline{\varphi}^{\mathrm{cor}} = 1 - \overline{\varphi}^{\mathrm{lip}}$	0.9684	0.9073

More significant digits are given than in statements in the text.

Eq. (41) (and also earlier Eqs. (16)–(18), (22), (37) and (39)) show that the concentration basis used for bound solute (per keratin mass, or per total keratin dispersion or tissue volume) does not affect the "off" (unbinding) rate constant. This outcome is consistent with the notion that the mean survival time of a bound solute molecule as an entity stuck to the surface of a keratin microfibril, and therefore the first-order kinetics of its detachment, would appear to be an attribute of the adsorption process independent of the volumetric distribution and number density of microfibrils. However, the "on" (binding) rate constant is strongly influenced by the concentration basis used (see factors labeled $f_{\mathrm{ultra}\to\mathrm{micro}}$ and $f_{\mathrm{micro}\to\mathrm{macro}}$ appearing in Eqs. (36), (38) and (40)).

Eq. (40) may be rewritten in a convenient alternate form by dividing both numerator and denominator by $\overline{\varphi}^{\mathrm{cor}}$, making use of Eq. (27) and substituting numerical values from Table 2 to arrive at

$$\overline{\overline{k}}_{\mathrm{on}}^{\mathrm{sc}} = \frac{1.37\,\phi^{\mathrm{ker}}\,k_{\mathrm{on},q,Q_{\mathrm{true}}}}{(\overline{\varphi}^{\mathrm{lip}}/\overline{\varphi}^{\mathrm{cor}})\overline{K}^{\mathrm{lip/w}} + 1 - \phi^{\mathrm{ker}}(1+\lambda)^2} = \frac{\text{numerator}}{\text{denominator}}$$
$$= \begin{cases} \dfrac{0.2641\,k_{\mathrm{on},q,Q_{\mathrm{true}}}}{0.0326\,\overline{K}^{\mathrm{lip/w}} + 1 - 0.1928\,(1+\lambda)^2} & (\text{fully hydrated}) \\ \dfrac{0.8280\,k_{\mathrm{on},q,Q_{\mathrm{true}}}}{0.1022\,\overline{K}^{\mathrm{lip/w}} + 1 - 0.6044\,(1+\lambda)^2} & (\text{partially hydrated}). \end{cases} \tag{42}$$

It is important to emphasize that the observable binding kinetics in skin reflects a volume average over the two phases making up the SC, embodied by the denominators in Eqs. (40) and (42), which include terms characterizing both corneocyte and lipid phases. In contrast, keratin binding experiments with a powdered substrate reflect the protein within the corneocyte phase only, embodied by the rate constant $k_{\mathrm{on},q,Q_{\mathrm{true}}}$ in the numerators.

Dependence of Macroscopic "On" (Binding) Rate Constant on Hydration State

Eq. (42) can be applied to calculate $\overline{\overline{k}}_{\mathrm{on}}^{\mathrm{sc}}$ for both partially and fully hydrated states of the SC. Figure 5 shows the ratio $(\overline{\overline{k}}_{\mathrm{on}}^{\mathrm{sc}})_{\text{partially hydrated}}/(\overline{\overline{k}}_{\mathrm{on}}^{\mathrm{sc}})_{\text{fully hydrated}}$ of the results implied by this calculation as a function of solute lipophilicity, quantified by $\log_{10}K^{\mathrm{o/w}}$, for three fixed values of the solute size, quantified by its molar volume V_{A} or radius a^{solute}. The key assumption underlying Figure 5 — that the intrinsic binding properties of keratin microfibrils are independent of hydration state — is commented on in the Discussion section. The usefulness of the graph lies in that it suggests how rate constants determined from in vitro experiments with either partially or fully hydrated states might translate to the in vivo conditions of ultimate interest. The broad conclusion is that $(\overline{\overline{k}}_{\mathrm{on}}^{\mathrm{sc}})_{\text{partially hydrated}}$ approaches roughly 7–11 times $(\overline{\overline{k}}_{\mathrm{on}}^{\mathrm{sc}})_{\text{fully hydrated}}$ in the limit of highly hydrophilic solutes over the size range considered, and the two rate constants become equal in the limit of highly lipophilic solutes.

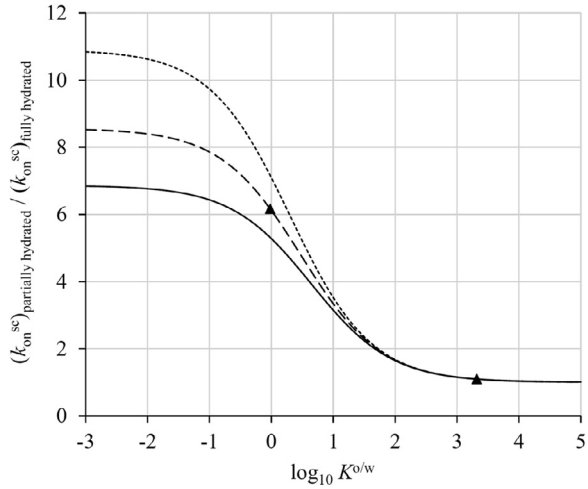

Figure 5. Ratio of macroscopically observable "on" (binding) rate constants $\bar{\bar{k}}_{on}^{sc}$ for partially to fully hydrated SC as a function of solute lipophilicity (quantified by $\log_{10}K^{o/w}$), as predicted by Eq. (42) and other equations listed in Table 3, for three fixed values of the solute size (quantified by its molar volume V_A or radius a^{solute}). Solid, dashed and dotted curves correspond to $V_A = 21$ cm^3/mol ($a^{solute} = 0.90$ Å, the size of water), $V_A = 168$ cm^3/mol ($a^{solute} = 3.14$ Å, the size of theophylline) and $V_A = 350$ cm^3/mol ($a^{solute} = 4.87$ Å, the size of testosterone), respectively. Filled triangles represent the examples of solutes theophylline ($\log_{10}K^{o/w} = -0.02$ on the dashed curve) and testosterone ($\log_{10}K^{o/w} = 3.32$ on the dotted curve) presented at the end of the Discussion section.

Dependence of Macroscopic "On" (Binding) Rate Constant on Lipophilicity

As opposed to the ratio comparing hydration states just discussed, a definitive statement of the absolute value of $\bar{\bar{k}}_{on}^{sc}$ for human SC must await experimental studies with this tissue or keratin deriving from it. Nevertheless, the preceding analysis makes it possible it to formulate useful speculations about human SC keratin based on Seif and Hansen's kinetic studies with BHH keratin.[10] Two facts serve as our starting point. The first is their kinetic characterization of BHH keratin embodied in either Eq. (34) or Eq. (35). The second is Hansen et al.'s[39] finding that

$$K_{eq,q,Q_{true}} = 10^{-0.6}\,(K_{eq,q,Q_{true}})_{BHH}$$
$$\text{or}\quad \frac{k_{on,q,Q_{true}}}{k_{off,q,Q_{true}}} = 10^{-0.6}\left(\frac{k_{on,q,Q_{true}}}{k_{off,q,Q_{true}}}\right)_{BHH}, \tag{43}$$

as noted above (cf. Eq. (33)). Here the equals signs (=) represent an average characterization of large datasets on human delipidized SC and callus keratin vis-à-vis BHH keratin, subject to scatter, as opposed to a literal mathematical equality applicable to any particular solute.

One might ask, how does it come to pass that the binding equilibrium constant for human SC keratin is $10^{0.6}$ (~ 4) times smaller than that for BHH keratin? Among the infinite set of possible explanations, a particularly simple case stands out: it might be that $k_{on,q,Q_{true}} = 10^{-0.6}(k_{on,q,Q_{true}})_{BHH}$ and $k_{off,q,Q_{true}} = (k_{off,q,Q_{true}})_{BHH}$, i.e., the "on" (binding) rate constant is ~ 4 times smaller, and the "off" (unbinding) rate constant is the same. The most general statement of such a relation would be

Case A ($k_{off,q,Q_{true}}$ for human SC keratin $= k_{off,q,Q_{true}}$ for BHH keratin):

$$k_{on,q,Q_{true}} = 10^{-0.6}\,\gamma\cdot(k_{on,q,Q_{true}})_{BHH} \tag{44a}$$

$$\text{and}\quad k_{off,q,Q_{true}} = \gamma\cdot(k_{off,q,Q_{true}})_{BHH}, \tag{44b}$$

where γ is an arbitrary positive number. Another intriguing possibility is to take Eq. (34) at face value as a characterization of relative unbinding rates of different solutes for keratins generally, so that it would apply equally to human SC keratin, i.e.,

Case B (relationship between $k_{off,q,Q_{true}}$ and $K_{eq,q,Q_{true}}$ is identical for human SC and BHH keratins):

$$\frac{k_{off,q,Q_{true}}}{\text{min}^{-1}} = \gamma\cdot\left[25.75 + 0.459\,K_{eq,q,Q_{true}}\right]^{-1}. \tag{45}$$

Again, this equation quantifies Seif and Hansen's[10] observation that the desorption rate decreases with increasing strength of equilibrium binding. The speculation here is that this equation might describe the effects of variations in $K_{eq,q,Q_{true}}$ arising from both solute lipophilicity *and type of keratin*. In both Eqs. (44) and (45) the factor γ allows for a possible adjustment of absolute values of rate constants for human SC vis-à-vis experimental data as they become available.

The two panels of Figure 6 show how the macroscopically observable binding rate constants are predicted to depend on $\log_{10}K^{o/w}$ based on Eqs. (41) and (42) for cases A and B, for three fixed values of the solute size. No adjustments of the absolute values are attempted ($\gamma = 1$). For case A $k_{off,q,Q_{true}}$ is calculated from Eq. (44b), with $(k_{off,q,Q_{true}})_{BHH}$ given by Eq. (35), whereas for case B $k_{off,q,Q_{true}}$ is calculated from Eq. (45), with $K_{eq,q,Q_{true}}$ given by Eq. (32). For both cases $k_{on,q,Q_{true}}$ is subsequently obtained as the product $K_{eq,q,Q_{true}} \times k_{off,q,Q_{true}}$ (see Eq. (19)), with $K_{eq,q,Q_{true}}$ given by Eq. (32). For both cases $k_{on,q,Q_{true}}$ is found to exhibit a pronounced maximum at an intermediate lipophilicity. Changing γ would change the magnitude of all the calculated values of $k_{on,q,Q_{true}}$, but would not alter the shape of the curve. Thus, the maximum seems to be a robust feature of the theory. At the current state of knowledge we regard case B as the more plausible of the two parameterizations of rate constants proposed above.

Discussion

The main results of our analysis are Eqs. (41) and (42) linking the macroscopically observable (volume-average) rate constants characterizing solute binding to keratin in human SC, and the keratin mass –based rate constants that could be measured in in vitro binding studies. In principle, these equations would allow results of such binding studies to be built into model-based predictions of transient dermal absorption outcomes. They would also allow fundamental ultrascopic kinetic parameters characterizing human SC keratin to be deduced from values of $\bar{\bar{k}}_{on}^{sc}$ and $\bar{\bar{k}}_{off}^{sc}$ fitted to the results of transient permeation and/or desorption experiments. Kinetic studies across a spectrum of solutes are called for to establish a broadly validated parameterization of $k_{off,q,Q_{true}}$ specific to human SC keratin for use with the theory presented here (cf. Eqs. (44b) and (45)). Such studies are the subject of ongoing research.

The real import of our analysis lies in its quantitative elucidation of variations in $\bar{\bar{k}}_{on}^{sc}$ that necessarily follow from variations in keratin density (i.e., the amount of keratin per unit volume) inside corneocytes at different states of hydration. Furthermore, without doing the math there would be no way to know that a maximum in $\bar{\bar{k}}_{on}^{sc}$ at an intermediate solute lipophilicity is a natural, logical consequence (i.e., homogenized or coarse-grained outcome) of the underlying microscopic physics. Thus, our analysis furnishes the theoretical framework needed to properly understand and interpret experimental kinetic studies. In this context Figures 5 and 6 can be regarded as presenting experimentally testable hypotheses. Any deviations from the trends they exhibit would suggest the involvement of a physicochemical factor additional to the average keratin density within corneocytes.

Ultra-to-Micro Homogenization of Binding Kinetics

The derivation of Eqs. (20)–(22) is presented in a self-contained way in the preliminary section titled "Fundamental Parameters and Mathematical Relationships..." above. We have checked that the same results are obtained by repurposing Nitsche and Frasch's theory[8] (asymptotic analysis of unit-cell eigenvalue problem characterizing time evolution of zeroth moment of solute distribution) to address the ultrascopic-to-microscopic homogenization. This check requires a generalization to surface (as opposed to volumetrically distributed) binding seen at the ultrascopic scale (theoretical calculations not shown). The derivation presented here represents a simpler way of arriving at these results.

Effects of Hydration

For highly lipophilic solutes $\overline{\varphi}^{\mathrm{lip}}\overline{K}^{\mathrm{lip/w}} \gg \overline{\varphi}^{\mathrm{cor}}\overline{K}^{\mathrm{cor/w}}$ in the denominator of Eq. (40). Also, owing to Eq. (27), $\overline{K}^{\mathrm{cor/w}}$ in the numerator cancels $1-\phi^{\mathrm{keratin}}(1+\lambda)^2$ in the denominator. Thus,

$$\overline{\overline{k}}^{\mathrm{sc}}_{\mathrm{on}} \sim \left(\frac{\overline{\varphi}^{\mathrm{cor}}}{\overline{\varphi}^{\mathrm{lip}}\overline{K}^{\mathrm{lip/w}}} \cdot \frac{\rho^{\mathrm{ker}}}{\rho^{\mathrm{w}}[\mathrm{v.c.}]} \cdot \phi^{\mathrm{ker}}\right) k_{\mathrm{on},q,Q_{\mathrm{true}}}. \tag{46}$$

Interpretation of the factor $\overline{\varphi}^{\mathrm{cor}}\phi^{\mathrm{ker}}/\varphi^{\mathrm{lip}}$ as

$$\frac{\overline{\varphi}^{\mathrm{cor}}\phi^{\mathrm{ker}}}{\overline{\varphi}^{\mathrm{lip}}} = \frac{\text{corneocyte vol.}}{\text{total SC vol.}} \cdot \frac{\text{keratin vol.}}{\text{corneocyte vol.}} \Big/ \frac{\text{lipid vol.}}{\text{total SC vol.}} = \frac{\text{keratin vol.}}{\text{lipid vol.}} \tag{47}$$

shows that it is, in fact, independent of the amount of water that hydrates the corneocytes. This logic explains why the curves in Figure 5 all asymptotically approach unity at large values of $\log_{10}K^{\mathrm{o/w}}$.

Figure 5 assumes that the intrinsic binding properties of keratin microfibrils are independent of hydration state. At higher concentrations of keratin (in particular, for partially hydrated SC), close proximity or contact of microfibrils might lead to effective occlusion of some binding sites, reducing the overall (surface– or mass–average) binding rate at a fixed value of κ_{on} for isolated microfibrils. Furthermore, as remarked by Hansen et al.[48] (p. 1385) citing Yadev et al,[18] "[i]t has been argued that with swelling keratin uncoils and exposes additional binding sites." Both mechanisms would tend to decrease the partially/fully hydrated ratio in Figure 5. However, as noted in the Introduction, the unfolding process is thought to be largely complete by the time the water content is 20–30 wt% (see Refs. 15 and 18 and references therein), and so would not affect the comparison between partially and fully hydrated states. Ultimately, the extent of these phenomena cannot be ascertained by theoretical argument, and should be informed by experiment.

Maximum in the Dependence of $\overline{\overline{k}}^{sc}_{on}$ Upon $\log_{10}K^{o/w}$

The most prominent feature of Figure 6 is the maximum in $\overline{\overline{k}}^{\mathrm{sc}}_{\mathrm{on}}$, the "on" (binding) rate constant observable in skin, at an intermediate value of $\log_{10}K^{\mathrm{o/w}}$. It results from an interesting interplay between the differing rates of increase of the numerator and denominator in Eq. (42) with increasing $K^{\mathrm{o/w}}$. As noted above, the numerator reflects the intrinsic kinetics of solute binding to protein within the corneocyte phase only, which would be observed in keratin binding experiments with a powdered substrate. The denominator reflects the volume averaging needed to describe the macroscopically observable outcome of the binding process as it plays out in the two-phase system considered as an effective continuum.

First, the ultrascopic "on" (binding) rate constant $k_{\mathrm{on},q,Q_{\mathrm{true}}}$ appearing in the numerator of Eq. (42) increases weakly with increasing $K^{\mathrm{o/w}}$. For example, according to Eq. (45) representing case B together with Eq. (19),

$$k_{\mathrm{on},q,Q_{\mathrm{true}}} = K_{\mathrm{eq},q,Q_{\mathrm{true}}}\, k_{\mathrm{off},q,Q_{\mathrm{true}}} = \gamma \cdot \frac{K_{\mathrm{eq},q,Q_{\mathrm{true}}} \cdot \mathrm{min}^{-1}}{25.75 + 0.459\, K_{\mathrm{eq},q,Q_{\mathrm{true}}}}, \tag{48}$$

in which we take $\gamma = 1$ (no adjustment of Seif and Hansen's correlation[10]). The binding equilibrium constant $K_{\mathrm{eq},q,Q_{\mathrm{true}}}$ increases with increasing $K^{\mathrm{o/w}}$, as $K^{\mathrm{o/w}}$ raised to the power 0.32 according to Eq. (32). Owing to the smallish exponent and because $K_{\mathrm{eq},q,Q_{\mathrm{true}}}$ appears in both the numerator and denominator in Eq. (48), the increase of the "on" (binding) rate constant $k_{\mathrm{on},q,Q_{\mathrm{true}}}$ (and therefore the numerator in Eq. (42)) is weak, and it asymptotically approaches the value $0.459^{-1} = 2.18$ for highly lipophilic solutes ($K^{\mathrm{o/w}} \gg 1$).

Second, the denominator in Eq. (42) also increases with increasing $K^{\mathrm{o/w}}$ owing to the first term containing $\overline{K}^{\mathrm{lip/w}}$. However, the character of the increase is different. For hydrophilic solutes (small values of $K^{\mathrm{o/w}}$ and therefore $\overline{K}^{\mathrm{lip/w}}$) the term containing $\overline{K}^{\mathrm{lip/w}}$ is negligible compared with $1-\phi^{\mathrm{ker}}(1+\lambda)^2$, making the denominator essentially constant. For lipophilic solutes (large values of $K^{\mathrm{o/w}}$ and therefore $\overline{K}^{\mathrm{lip/w}}$) this term becomes dominant, making the denominator increase strongly, as $K^{\mathrm{o/w}}$ raised to the power 0.67 according Eq. (26).

Figure 7 shows the numerator and denominator in Eq. (42) separately as functions of $\log_{10}K^{\mathrm{o/w}}$, illustrating the trends described above for both. For definiteness, the curves shown are calculated for partially hydrated SC and for a solute having the size of tracer water ($V_{\mathrm{A}} = 21$ cm^3/mol, $a^{\mathrm{solute}} = 0.90$ Å, $\lambda = 0.026$), although any other size could also have been used. For small values of $K^{\mathrm{o/w}}$ (left side of Figs. 6 and 7) the weak increase in the numerator dominates over the negligible increase in the denominator, causing $\overline{\overline{k}}^{\mathrm{sc}}_{\mathrm{on}}$ to increase with increasing $K^{\mathrm{o/w}}$. For large values of $K^{\mathrm{o/w}}$ (right side of Figs. 6 and 7) the strong increase in the denominator overwhelms the weak increase in the numerator, causing $\overline{\overline{k}}^{\mathrm{sc}}_{\mathrm{on}}$ to decrease, i.e., come back down. This competition between the numerator in Eq. (42) (reflecting intrinsic kinetics of solute-keratin binding) and the denominator (embodying the volume average over corneocyte and lipid phases needed to characterize the SC macroscopically) is what produces the maximum in $\overline{\overline{k}}^{\mathrm{sc}}_{\mathrm{on}}$ at an intermediate value of $K^{\mathrm{o/w}}$.

It is worth noting that the maximum at an intermediate value of $\log_{10}K^{\mathrm{o/w}}$ is not unique to $\overline{\overline{k}}^{\mathrm{sc}}_{\mathrm{on}}$, i.e., to binding kinetics. The macroscopically observable binding equilibrium constant obtained by taking the ratio of Eqs. (42) to (41), i.e.,

$$\overline{\overline{K}}^{\mathrm{sc}}_{\mathrm{eq}} = \frac{\overline{\overline{k}}^{\mathrm{sc}}_{\mathrm{on}}}{\overline{\overline{k}}^{\mathrm{sc}}_{\mathrm{off}}} = \begin{cases} \dfrac{0.2641\, K_{\mathrm{eq},q,Q_{\mathrm{true}}}}{0.0326\, \overline{K}^{\mathrm{lip/w}} + 1 - 0.1928\,(1+\lambda)^2} & \text{(fully hydrated)} \\ \dfrac{0.8280\, K_{\mathrm{eq},q,Q_{\mathrm{true}}}}{0.1022\, \overline{K}^{\mathrm{lip/w}} + 1 - 0.6044\,(1+\lambda)^2} & \text{(partially hydrated)}, \end{cases} \tag{49}$$

also exhibits this feature, as shown in Fig. 8, for the same basic reason as that enunciated for $\overline{\overline{k}}^{\mathrm{sc}}_{\mathrm{on}}$.

Other Binding Sites

Hansen et al.[48] allow for a contribution to solute–protein binding from the cornified cell envelope[41,54,55] (their Ω_{cpe} compartment) in addition to intracellular keratin, although it is considered only in terms of a Langmuir isotherm (equilibrium binding, no kinetics), and only by parametric study given the complete lack of experimental data on its binding properties. Our analysis does not address this possible bound solute compartment because any theoretical results derived would be entirely speculative at the current state of knowledge. We can, however, estimate the mass of cornified cell envelope (CE) proteins relative to intracellular keratins. Assuming the CE to be

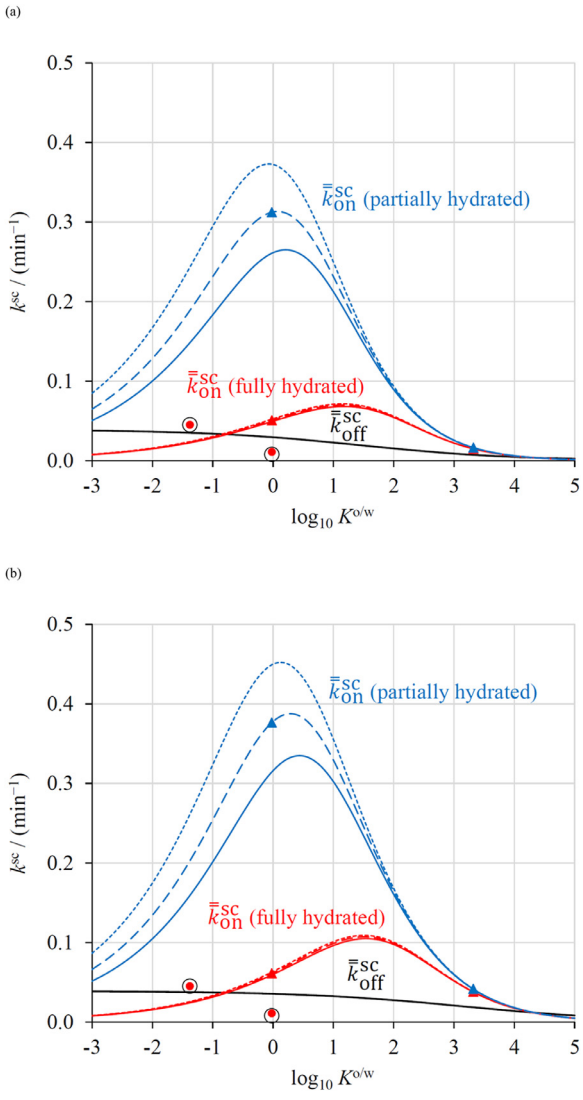

Figure 6. Macroscopically observable rate constants $\bar{\bar{k}}^{sc}_{on}$ and $\bar{\bar{k}}^{sc}_{off}$ for human SC as functions of solute lipophilicity (quantified by $\log_{10}K^{o/w}$), as predicted by Eq. (42) and other equations listed in Table 3, for three fixed values of the solute size (quantified by its molar volume V_A or radius a^{solute}). Panels (a) and (b) represent cases A (see Eq. (44)) and B (see Eq. (45)) discussed in the text, respectively. Significance of solid, dashed and dotted curves, as well as filled triangles, is exactly the same as for Figure 5. Red, blue and black curves represent $\bar{\bar{k}}^{sc}_{on}$ for the fully hydrated state, $\bar{\bar{k}}^{sc}_{on}$ for the partially hydrated state, and $\bar{\bar{k}}^{sc}_{off}$ (the same for both states), respectively. Red filled circles and black open circles represent experimental determinations of $\bar{\bar{k}}^{sc}_{on}$ and $\bar{\bar{k}}^{sc}_{off}$, respectively, reported for water[7] ($\log_{10}K^{o/w} = -1.38$) and theophylline[9] ($\log_{10}K^{o/w} = -0.02$). (For interpretation of the references to colour in this figure legend, the reader is referred to the web version of this article.)

15–20 nm thick and to completely encase a 40 μm diameter disk-shaped corneocyte having a thickness of 0.8 μm, the volume ratio of CE to corneocyte interior is on the order of 1:25 to 1:19. If we take the protein volume fraction of the CE to be 0.8 and that of the partially hydrated corneocyte interior to be 0.6044 (Table 2) and (furthermore consider the protein densities to be equal, then the mass ratio of CE proteins to intracellular keratin would be 1:19 to 1:14. Surface area available for exogenous solute binding may slant even more heavily towards intracellular keratin due to the higher CE protein density and the fact that acylceramides are covalently bound to the CE exterior and keratins to the CE interior. Consequently we would expect the contribution of CE proteins to solute binding by SC proteins to be no higher than 5–7% of the total.

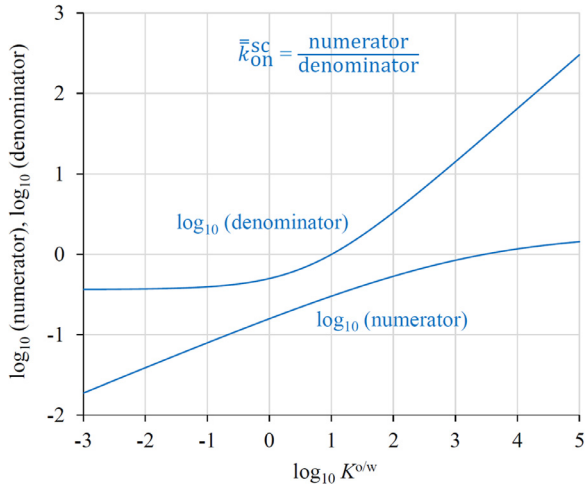

Figure 7. Numerator and denominator in Eq. (42) as functions of solute lipophilicity (quantified by $\log_{10}K^{o/w}$). The curves shown correspond to the solid blue curve in Figure 6(b), i.e., partially hydrated SC parameterized according to case B (see Eq. (45)) with solute molar volume fixed at the value $V_A = 21$ cm^3/mol.

Comparison with Experimental Data

Figure 6 includes the only two available data points for $\bar{\bar{k}}^{sc}_{on}$ and $\bar{\bar{k}}^{sc}_{off}$, determined by fitting permeation and/or desorption transients measured with fully hydrated human SC for water[7] and theophylline.[9] Water represents an exceptional case because "the phenomenon of keratin binding simply establishes two states for the water in the corneocyte phase; it does not involve a favorable bound state increasing corneocyte-phase holdup" of another solute molecule.[43] Therefore, our analysis does not strictly apply to water, and the datum for it is included only as an order-of-magnitude indicator of binding rate constants for a hydrophilic solute.

Frasch et al.'s best-fit value $\bar{\bar{k}}^{sc}_{off} = (0.466 \pm 0.147)\ h^{-1} = (0.0078 \pm 0.0025)\ min^{-1}$ for theophylline is smaller than the value $(25.75)^{-1}$ min^{-1} = 0.039 min^{-1} implied by Eqs. (34) and (35) for a hydrophilic solute for BHH keratin. However, the ratio $\bar{\bar{k}}^{sc}_{on}/\bar{\bar{k}}^{sc}_{off} = 1.40$ measured

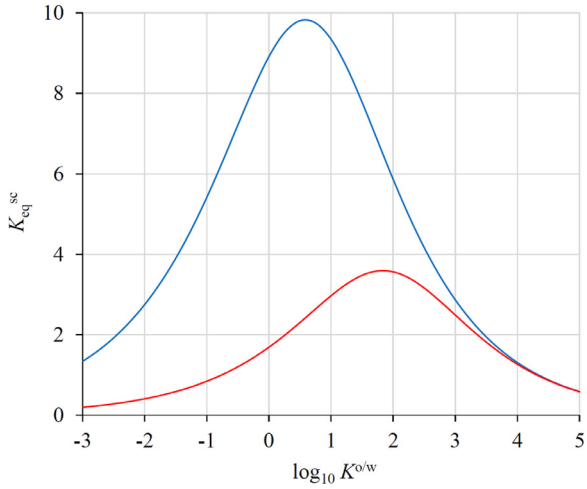

Figure 8. Macroscopically observable binding equilibrium constant $\bar{\bar{K}}^{sc}_{eq} \equiv \bar{\bar{k}}^{sc}_{on}/\bar{\bar{k}}^{sc}_{off}$ as a function of solute lipophilicity (quantified by $\log_{10}K^{o/w}$), as predicted by Eq. (49) and other equations listed in Table 3. The blue curve corresponds to the example considered in Figure 7, namely partially hydrated SC with solute molar volume fixed at the value $V_A = 21$ cm^3/mol. The red curve shown for comparison corresponds to fully hydrated SC with the same value of V_A. (For interpretation of the references to colour in this figure legend, the reader is referred to the web version of this article.)

Table 3
Summary of Equations Needed to Estimate the Macroscopically Observable (Volume-Average) Rate Constants $\overline{\overline{k}}^{sc}_{on}$ and $\overline{\overline{k}}^{sc}_{off}$ Characterizing Solute Binding to Keratin in Human SC.

Property	Equation	Eq. no. in text	Notes
SC lipid/water partition coefficient	$\log_{10}\overline{K}^{lip/w} = 0.12 + 0.67\ \log_{10}K^{o/w}$	(26)	a
Solute radius	$a^{solute} = \begin{cases} (0.145\ \text{Å})(V_A)^{0.6} & \text{if } V_A \le 445.2, \\ (0.735\ \text{Å})(V_A)^{1/3} & \text{if } V_A > 445.2 \end{cases}$	(28)	
Ratio of solute to keratin microfibril radii	$\lambda = a^{solute}/(35\ \text{Å})$	(6)	
Ultrascopic binding equilibrium constant	$\log_{10}K^{ker}_{eq} = 0.73 + 0.32\ \log_{10}K^{o/w}$	(32)	a, b
Ultrascopic "off" (unbinding) rate constant (case A estimate)	$k^{ker}_{off} = \dfrac{\gamma \cdot \text{min}^{-1}}{25.75 + 8.35\,(K^{o/w})^{0.34}}$	(35), (44b)	b, c
Ultrascopic "off" (unbinding) rate constant (case B estimate)	$k^{ker}_{off} = \dfrac{\gamma \cdot \text{min}^{-1}}{25.75 + 0.459\ K^{ker}_{eq}}$	(45)	b, c
Ultrascopic "on" (binding) rate constant	$k^{ker}_{on} = K^{ker}_{eq}\ k^{ker}_{off}$	(19)	b
Macroscopic "on" (binding) rate constant for fully hydrated SC	$\overline{\overline{k}}^{sc}_{on} = \dfrac{0.2641\ k^{ker}_{on}}{0.0326\ \overline{K}^{lip/w} + 1 - 0.1928\ (1+\lambda)^2}$	(42)	b
Macroscopic "on" (binding) rate constant for partially hydrated SC	$\overline{\overline{k}}^{sc}_{on} = \dfrac{0.8280\ k^{ker}_{on}}{0.1022\ \overline{K}^{lip/w} + 1 - 0.6044\ (1+\lambda)^2}$	(42)	b
Macroscopic "off" (unbinding) rate constant (same for fully and partially hydrated SC)	$\overline{\overline{k}}^{sc}_{off} = k^{ker}_{off}$	(41)	b

Two input parameters are needed for any solute. The first is $\log_{10}$ of the octanol/water partition coefficient ($\log_{10}K^{o/w}$), which can be obtained from the Estimation Program Interface (EPI) Suite, U.S. Environmental Protection Agency[49] accessed through ChemSpider.[50] The second is the solute's molar volume as a liquid at its normal boiling point in units of cm^3/mol (V_A), which is estimated using Schroeder's method (see Wang et al.'s[25] Eq. (B3) and following text, or Poling et al.'s[53] Eq. (4-10.1) on their p. 4.33).

[a] This equation could be replaced by any preferred variant represented in Table 1.

[b] This entry uses simplified notation for the ultrascopic parameters replacing the symbols $K_{eq,q,Q_{true}}$, $k_{on,q,Q_{true}}$ and $k_{off,q,Q_{true}}$ with K^{ker}_{eq}, k^{ker}_{on} and k^{ker}_{off}, respectively.

[c] At the current state of knowledge we suggest refraining from making any adjustments to the correlations given by Seif and Hansen[10] (i.e., suggest setting $\gamma = 1$), and regard case B as the more plausible of the two parameterizations of k^{ker}_{off}.

in an independent binding experiment, which was used to properly constrain the permeation data fitting, is matched reasonably well by the value of 1.72 implied by Eqs. (19), (32), (41) and (42) for fully hydrated SC (see Fig. 6). Co-fitting of a binding rate constant and a diffusion coefficient to transient permeation data is generally subject to some uncertainty, because many combinations of parameters might offer reasonable fits.

All told, the match between the very limited data and theory is at the order-of-magnitude level only, although within the observed level of scatter for equations such as Eq. (32) (cf. Hansen et al.'s[39] Fig. 3 and Hansen et al.'s[47] Fig. 4). More comprehensive experimental characterization of human SC keratin binding kinetics is called for to establish solute lipophilicity and SC hydration state dependencies speculated on in this paper. Our analysis establishes the variations in $\overline{\overline{k}}^{sc}_{on}$ logically attributable to variations in the amount of keratin per unit volume in the SC, barring intervention of other physicochemical factors.

Upshot, Examples, and Significance for Topical and Transdermal Therapeutics

Table 3 summarizes all the equations needed to estimate $\overline{\overline{k}}^{sc}_{on}$ and $\overline{\overline{k}}^{sc}_{off}$ based on our analysis. The presentation utilizes the simplified symbols K^{ker}_{eq}, k^{ker}_{on} and k^{ker}_{off} for the ultrascopic binding equilibrium and rate constants in lieu of $K_{eq,q,Q_{true}}$, $k_{on,q,Q_{true}}$ and $k_{off,q,Q_{true}}$, respectively (see Fig. 4). These constants appear in the binding isotherm $q = K^{ker}_{eq}Q_{true} = (k^{ker}_{on}/k^{ker}_{off})Q_{true}$ and rate expression $dq/dt = k^{ker}_{on}Q_{true} - k^{ker}_{off}q$ that would be determined in a keratin binding study such as Seif and Hansen's[10] (cf. Eqs. (11) and (17)).

The filled triangles in Figures 5 and 6 represent the solutes theophylline ($\log_{10}K^{o/w} = -0.02$, $V_A = 168\ cm^3/mol$) and testosterone ($\log_{10}K^{o/w} = 3.32$, $V_A = 350\ cm^3/mol$) considered as illustrative examples, for which the equations in Table 3 yield the calculated results listed in Table 4. These examples may be used to check any computational implementation of Table 3.

Table 4
Calculated Properties of the Solutes Theophylline ($\log_{10}K^{o/w} = -0.02$, $V_A = 168\ cm^3/mol$) and Testosterone ($\log_{10}K^{o/w} = 3.32$, $V_A = 350\ cm^3/mol$) Presented as Examples Illustrating the Use of the Equations Listed in Table 3.

Property	Theophylline		Testosterone	
	Value for case A	Value for case B	Value for case A	Value for case B
$\overline{K}^{lip/w}$	1.28		2.21×10^2	
a^{solute} (Å)	3.14		4.87	
λ	0.090		0.139	
K^{ker}_{eq}	5.29		6.20×10^1	
k^{ker}_{off} (min^{-1})	2.94×10^{-2}	3.55×10^{-2}	7.24×10^{-3}	1.84×10^{-2}
k^{ker}_{on} (min^{-1})	1.56×10^{-1}	1.88×10^{-1}	4.49×10^{-1}	1.14
$\overline{\overline{k}}^{sc}_{on}$ fully hydrated (min^{-1})	5.06×10^{-2}	6.10×10^{-2}	1.49×10^{-2}	3.79×10^{-2}
$\overline{\overline{k}}^{sc}_{on}$ partially hydrated (min^{-1})	3.12×10^{-1}	3.77×10^{-1}	1.63×10^{-2}	4.15×10^{-2}
$\overline{\overline{k}}^{sc}_{off}$ both fully and partially hydrated (min^{-1})	2.94×10^{-2}	3.55×10^{-2}	7.24×10^{-3}	1.84×10^{-2}

The significance of our analysis for topical and transdermal therapeutics is that it directly facilitates the incorporation of transient drug binding to the substantial amount of keratin within corneocytes into model predictions of dermal absorption outcomes. It does so specifically by providing order-of-magnitude estimates of the rate constants appearing in the binding terms of the macroscopic equations

$$\begin{aligned} \partial\overline{\overline{C}}^{sc}/\partial t &= \partial^2\overline{\overline{D}}^{sc}/\partial z^2 - \Big(\underbrace{\overline{\overline{k}}_{on}^{sc}\overline{\overline{C}}^{sc} - \overline{\overline{k}}_{off}^{sc}\overline{\overline{B}}^{sc}}_{\text{binding terms}}\Big), \\ \partial\overline{\overline{B}}^{sc}/\partial t &= \underbrace{\overline{\overline{k}}_{on}^{sc}\overline{\overline{C}}^{sc} - \overline{\overline{k}}_{off}^{sc}\overline{\overline{B}}^{sc}}_{\text{binding terms}} \end{aligned} \tag{50}$$

describing solute transport in the SC barrier layer of skin. These terms are missing from the SC transport models embedded in existing dermal absorption calculators, such as NIOSH's Finite Dose Skin Permeation Calculator[22] and the skin permeation model built into the open-source PK-Sim® platform for physiologically based pharmacokinetic modeling.[23] Transient keratin binding is known to substantially influence permeation and desorption transients, e.g. to the extent of causing major changes in parameters fitted to data that will be used to make subsequent predictions.[7,9] However, until now there has been no direct logical link between the rate constants $\overline{\overline{k}}_{on}^{sc}$ and $\overline{\overline{k}}_{off}^{sc}$ needed to include this binding in dermal absorption models on the one hand, and the results of in vitro keratin binding studies on the other hand. Equally lacking has been any broad basis for understanding the trends that these rate constants might be expected to exhibit as functions of drug lipophilicity, and parameterizing them in a reasonable way based on existing knowledge. Our analysis fills these needs, and provides a framework for understanding and unifying future experimental studies illuminating transient keratin binding in human SC.

The higher binding rate constants for partially vis-à-vis fully hydrated SC (see Fig. 5, and blue versus red curves in Fig. 6) suggests that drug–keratin binding should equilibrate faster in partially hydrated skin than in fully hydrated skin. The maximum in the dependence of $\overline{\overline{k}}_{on}^{sc}$ upon $\log_{10}K^{o/w}$ additionally suggests that — for a given hydration state — drug–keratin binding might equilibrate fastest for drugs for which $0 \lesssim \log_{10}K^{o/w} \lesssim 2$. This maximum was not evident in Nitsche and Frasch's previous analysis[8] because neither Seif and Hansen's binding kinetics dataset[10] nor the ultrascopic-to-microscopic homogenization needed for its broad application to dermal absorption existed at the time of writing.

Kinetics of solute binding to keratin in skin has long been recognized as the SC reservoir, as reviewed by Seif and Hansen.[10] The new framework developed here allows quantitative estimation of this property, and the associated time scale for release from the tissue, based on molecular size and lipophilicity of the permeating solute. We encourage others to test and better parameterize these predictions.

Declaration of Competing Interest

None.

Acknowledgments

The authors gratefully acknowledge funding of this work from the U.S. National Science Foundation (NSF) GOALI program under grant numbers 2124495 and 2124542 (CBET). J.M.N. gratefully acknowledges useful discussions with Dr. H. Frederick Frasch, and partial support from the U.S. National Institute for Occupational Safety and Health (NIOSH), in early stages of this work. The conclusions drawn here reflect the opinions of the authors and have not been endorsed by NSF or NIOSH.

References

1. Hadgraft J, Guy R H. Feasibility assessment in topical and transdermal delivery: mathematical models and in vitro studies, Chapter 1. In: Guy RH, Hadgraft J, eds. *Transdermal Drug Delivery*. New York: Marcel Dekker; 2002:1–23.
2. Kalia YN, Guy RH. Modeling transdermal drug release. *Adv Drug Deliv Rev*. 2001;48(2-3):159–172. https://doi.org/10.1016/s0169-409x(01)00113-2.
3. Prausnitz MR, Mitragotri S, Langer R. Current status and future potential of transdermal drug delivery. *Nat Rev Drug Discov*. 2004;3(2):115–124. https://doi.org/10.1038/nrd1304.
4. Van de Sandt JJM, Dellarco M, Van Hemmen JJ. From dermal exposure to internal dose. *J Expo Sci Environ Epidemiol*. 2007;17:S38–S47. https://doi.org/10.1038/sj.jes.7500579.
5. Frasch HF, Dotson GS, Bunge AL, et al. Analysis of finite dose dermal absorption data: implications for dermal exposure assessment. *J Expo Sci Environ Epidemiol*. 2014;24(1):65–73.
6. Exposure assessment tools by routes – dermal, U.S. Environmental Protection Agency. Available at: https://www.epa.gov/expobox/exposure-assessment-tools-routes-dermal. Accessed October 10, 2021.
7. Anissimov YG, Roberts MS. Diffusion modelling of percutaneous absorption kinetics: 4. Effects of a slow equilibration process within stratum corneum on absorption and desorption kinetics. *J Pharm Sci*. 2009;98(2):772–781. https://doi.org/10.1002/jps.21461.
8. Nitsche JM, Frasch HF. Dynamics of diffusion with reversible binding in microscopically heterogeneous membranes: general theory and applications to dermal penetration. *Chem Eng Sci*. 2011;66(10):2019–2041. https://doi.org/10.1016/j.ces.2011.01.008.
9. Frasch HF, Barbero AM, Hettick JM, Nitsche JM. Tissue binding affects the kinetics of theophylline diffusion through the stratum corneum barrier layer of skin. *J Pharm Sci*. 2011;100(7):2989–2995. https://doi.org/10.1002/jps.22489.
10. Seif S, Hansen S. Measuring the stratum corneum reservoir: desorption kinetics from keratin. *J Pharm Sci*. 2012;101(10):3718–3728. https://doi.org/10.1038/jes.2013.23.
11. Grégoire S, Sorrell I, Lange D, et al. Cosmetics Europe evaluation of 6 *in silico* skin penetration models. *Comput Toxicol*. 2021;19:100177. https://doi.org/10.1016/j.comtox.2021.100177.
12. Scheuplein RJ, Blank IH. Permeability of the skin. *Physiol Rev*. 1971;51(4):702–747.
13. Wang B, Yang W, McKittrick J, Meyers MA. Keratin: structure, mechanical properties, occurrence in biological organisms, and efforts at bioinspiration. *Prog Mater Sci*. 2016;76:229–318. https://doi.org/10.1016/j.pmatsci.2015.06.001.
14. Robbins CR, Fernee KM. Some observations on the swelling of human epidermal membrane. *J Soc Cosmet Chem*. 1983;34(1):21–34.
15. Kasting GB, Barai ND. Equilibrium water sorption in human stratum corneum. *J Pharm Sci*. 2003;92(8):1624–1631. https://doi.org/10.1002/jps.10420.
16. Cassie ABD. Absorption of water by wool. *Trans Faraday Soc*. 1945;41:458–464.
17. Blank IH. Factors which influence the water content of the stratum corneum. *J Invest Dermatol*. 1952;18(6):433–440. https://doi.org/10.1038/jid.1952.52.
18. Yadav S, Pinto NG, Kasting GB. Thermodynamics of water interaction with human stratum corneum I: measurement by isothermal calorimetry. *J Pharm Sci*. 2007;96(6):1585–1597. https://doi.org/10.1002/jps.20781 .
19. Matoltsy AG, Parakkal PF. Keratinization, Chapter 5. In: Zelickson AS, ed. *Ultrastructure of Normal and Abnormal Skin*. Philadelphia: Lea & Febiger; 1967:76–104.
20. Dancik Y, Miller MA, Jaworska J, Kasting GB. Design and performance of a spreadsheet-based model for estimating bioavailability of chemicals from dermal exposure. *Adv Drug Deliv Rev*. 2013;65(2):221–236. https://doi.org/10.1016/j.addr.2012.01.006.
21. Miller MA, Kasting GB. A spreadsheet-based method for simultaneously estimating the disposition of multiple ingredients applied to skin. *J Pharm Sci*. 2015;104(6):2047–2055. https://doi.org/10.1002/jps.24450.
22. Fedorowicz A, Milller MA, Kasting GB, Frasch HF. Finite dose skin permeation calculator, U.S. National institute for occupational safety and health. Available at: https://www.cdc.gov/niosh/topics/skin/finiteskinpermcalc.html. Accessed October 10, 2021.
23. Open systems pharmacology, skin permeation model. Available at: https://github.com/Open-Systems-Pharmacology/Skin-permeation-model. Accessed October 10, 2021.
24. Wang T-F, Kasting GB, Nitsche JM. A multiphase microscopic diffusion model for stratum corneum permeability. I. Formulation, solution, and illustrative results for representative compounds. *J Pharm Sci*. 2006;95(3):620–648. https://doi.org/10.1002/jps.20509.
25. Wang T-F, Kasting GB, Nitsche JM. A multiphase microscopic diffusion model for stratum corneum permeability. II. Estimation of physicochemical parameters, and application to a large permeability database. *J Pharm Sci*. 2007;96(11):3024–3051. https://doi.org/10.1002/jps.20883.
26. Barbero AM, Frasch HF. Effect of stratum corneum heterogeneity, anisotropy, asymmetry and follicular pathway on transdermal penetration. *J Control Release*. 2017;260:234–246. https://doi.org/10.1016/j.jconrel.2017.05.034.
27. Nitsche LC, Kasting GB, Nitsche JM. Microscopic models of drug/chemical diffusion through the skin barrier: effects of diffusional anisotropy of the intercellular lipid. *J Pharm Sci*. 2019;108(5):1692–1712. https://doi.org/10.1016/j.xphs.2018.11.014.
28. Wang J, Nitsche JM, Kasting GB, Wittum G, Naegel A. Transdermal and lateral effective diffusivities for drug transport in stratum corneum from a microscopic anisotropic diffusion model. Unpublished data. 2021.
29. Flynn GL. Mechanism of percutaneous absorption from physicochemical evidence. In: Bronaugh RL, Maibach HI, eds. *Percutaneous Absorption: Mechanism–Methodology–Drug Delivery*. New York: Marcel Dekker; 1985:17–42.

30. Johnson ME, Blankschtein D, Langer R. Evaluation of solute permeation through the stratum corneum: lateral bilayer diffusion as the primary transport mechanism. *J Pharm Sci*. 1997;86(10):1162–1172. https://doi.org/10.1021/js960198e.
31. Buchwald P, Bodor N. A simple, predictive, structure-based skin permeability model. *J Pharm Pharmacol*. 2001;53(8):1087–1098. https://doi.org/10.1211/0022357011776478.
32. Barbero AM, Frasch HF. Transcellular route of diffusion through stratum corneum: results from finite element models. *J Pharm Sci*. 2006;95(10):2186–2194. https://doi.org/10.1002/jps.20695.
33. Johnson ME, Berk DA, Blankschtein D, Golan DE, Jain RK, Langer RS. Lateral diffusion of small compounds in human stratum corneum and model lipid bilayer systems. *Biophys J*. 1996;71(5):2656–2668. https://doi.org/10.1016/S0006-3495(96)79457-2.
34. Selzer D, Hahn T, Naegel A, et al. Finite dose skin mass balance including the lateral part: comparison between experiment, pharmacokinetic modeling and diffusion models. *J Control Release*. 2013;165(2):119–128. https://doi.org/10.1016/j.jconrel.2012.10.009.
35. Zhang Q, Saad P, Mao G, et al. Infrared spectroscopic imaging tracks lateral distribution in human stratum corneum. *Pharm Res*. 2014;31(10):2762–2773. https://doi.org/10.1007/s11095-014-1373-8.
36. Rush AK, Miller MA, Smith ED 3rd, Kasting GB. A quantitative radioluminographic imaging method for evaluating lateral diffusion rates in skin. *J Control Release*. 2015;216:1–8. https://doi.org/10.1016/j.jconrel.2015.07.032.
37. Miller MA, Yu F, Kim K-I, Kasting GB. Uptake and desorption of hydrophilic compounds from human stratum corneum. *J Control Release*. 2017;261:307–317. https://doi.org/10.1016/j.jconrel.2017.06.015.
38. Kasting GB, Yu F. A geometrical model for diffusion of hydrophilic compounds in human stratum corneum. *Math Biosci*. 2018;300:55–63. https://doi.org/10.1016/j.mbs.2018.03.010.
39. Hansen S, Selzer D, Schaefer UF, Kasting GB. An extended database of keratin binding. *J Pharm Sci*. 2011;100(5):1712–1726. https://doi.org/10.1002/jps.22396.
40. Perkins SJ. Protein volumes and hydration effects. The calculations of partial specific volumes, neutron scattering matchpoints and 280-nm absorption coefficients for proteins and glycoproteins from amino acid sequences. *Eur J Biochem*. 1986;157(1):169–180. https://doi.org/10.1111/j.1432-1033.1986.tb09653.x.
41. Jarnik M, Simon MN, Steven AC. Cornified cell envelope assembly: a model based on electron microscopic determinations of thickness and projected density. *J Cell Sci*. 1998;111(8):1051–1060. https://doi.org/10.1242/jcs.111.8.1051.
42. Fischer H, Polikarpov I, Craievich AF. Average protein density is a molecular-weight-dependent function. *Protein Sci*. 2004;13(10):2825–2828. https://doi.org/10.1110/ps.04688204.
43. Nitsche JM, Wang T-F, Kasting GB. A two-phase analysis of solute partitioning into the stratum corneum. *J Pharm Sci*. 2006;95(3):649–666. https://doi.org/10.1002/jps.20549.
44. Raykar PV, Fung M-C, Anderson BD. The role of protein and lipid domains in the uptake of solutes by human stratum corneum. *Pharm Res*. 1988;5(3):140–150. https://doi.org/10.1023/a:1015956705293.
45. Anderson BD, Raykar PV. Solute structure-permeability relationships in human stratum corneum. *J Invest Dermatol*. 1989;93(2):280–286. https://doi.org/10.1111/1523-1747.ep12277592.
46. Wang L, Chen L, Lian G, Han L. Determination of partition and binding properties of solutes to stratum corneum. *Int J Pharm*. 2010;398(1-2):114–122. https://doi.org/10.1016/j.ijpharm.2010.07.035.
47. Hansen S, Lehr C-M, Schaefer UF. Improved input parameters for diffusion models of skin absorption. *Adv Drug Deliv Rev*. 2013;65(2):251–264. https://doi.org/10.1016/j.addr.2012.04.011.
48. Hansen S, Naegel A, Heisig M, et al. The role of corneocytes in skin transport revised—a combined computational and experimental approach. *Pharm Res*. 2009;26(6):1379–1397. https://doi.org/10.1007/s11095-009-9849-7.
49. Estimation program interface (EPI) suite. Washington, D.C.: U.S. Environmental Protection Agency. Available at: https://www.epa.gov/tsca-screening-tools/epi-suitetm-estimation-program-interface. Accessed October 10, 2021.
50. ChemSpider. Search and share chemistry. Cambridge, UK: Royal Society of Chemistry. Available at: http://www.chemspider.com. Accessed October 10, 2021.
51. Mitragotri S. A theoretical analysis of permeation of small hydrophobic solutes across the stratum corneum based on scaled particle theory. *J Pharm Sci*. 2002;91(3):744–752. https://doi.org/10.1002/jps.10048.
52. Nitsche JM, Kasting GB. How predictable are human stratum corneum lipid/water partition coefficients? Assessment and useful correlations for dermal absorption. *J Pharm Sci*. 2018;107(2):727–738. https://doi.org/10.1016/j.xphs.2017.07.026.
53. Poling BE, Prausnitz JM, O'Connell JP. *The Properties of Gases and Liquids*. 5th ed. New York: McGraw-Hill; 2001.
54. Steinert PM, Marekov LN. The proteins elafin, filaggrin, keratin intermediate filaments, loricrin, and small proline-rich proteins 1 and 2 are isopeptide cross-linked components of the human epidermal cornified cell envelope. *J Biol Chem*. 1995;270(30):17702–17711. https://doi.org/10.1074/jbc.270.30.17702.
55. Kalinin A, Marekov LN, Steinert PM. Assembly of the epidermal cornified cell envelope. *J Cell Sci*. 2001;114(17):3069–3070. https://doi.org/10.1242/jcs.114.17.3069.